J. Dobrić, N. Gluhović, Ivanović J, Rossi B. “Design procedures for cold-formed stainless steel built-up columns assembled from equal-leg angles” Journal of Constructional Steel Research, Volume 212, January 2024, 108263, https://doi.org/10.1016/j.jcsr.2023.108263.

Design procedures for cold-formed stainless steel built-up columns assembled from equal-leg angles

Jelena Dobrić[a,*], Nina Gluhović[a], Jovana Ivanović[a], Barbara Rossi[b]

[a] University of Belgrade, Faculty of Civil Engineering, Serbia

[b] University of Oxford, Department of Engineering Science, Oxford Sustainable Metal Structures Research Group, Oxford, United Kingdom

[*]Corresponding author: jelena@imk.grf.bg.ac.rs

Abstract

In this paper, the structural behaviour of cold-formed stainless steel (CFSS) built-up T- and cruciform-section columns is studied experimentally and numerically, and the effect of discrete fasteners on their flexural and torsional rigidity is considered. To build the singly symmetrical built-up T-section columns, two equal-leg angle sections made of lean-duplex grade EN 1.4162 were assembled back-to-back. The doubly symmetrical built-up cruciform-section columns were composed of four star-oriented equal-leg angle sections made of austenitic grade EN 1.4301. They were connected using M8 bolts of class 8.8. Two pin-ended built-up T-section columns with length of 1000 mm, and four built-up cruciform-section columns with lengths of 600 mm and 2400 mm with semi-rigid support conditions, were tested under pure axial compression. As observed in the tests, built-up T-section columns experienced flexural-torsional buckling failure, whereas built-up cruciform-section columns failed in torsional buckling mode. Finite element models were validated against the conducted experiments and used to perform a parametric study of the structural behaviour of CFSS built-up T- and cruciform-section columns. The study included the column length, cross-sectional dimensions and bolt spacing as variables. The experimental and numerical data, i.e., the column strengths and failure modes, were compared against the results obtained based on the European and North American Specifications alongside a recent method established for cold-formed carbon steel equivalents and based on the Direct Strength Method (DSM). It is shown that the DSM-based approach predicts the ultimate buckling resistances of the considered built-up columns more accurately than the available codified design methods.

Keywords

Stainless steel; Built-up columns; Discrete fasteners; Shear stiffness; Flexural-torsional buckling; Torsional buckling.

1 Introduction

Cold-formed steel (CFS) members, primarily owing to their smaller weight compared to their conventional hot-rolled and welded counterparts, are being increasingly implemented as parts of primary structural systems. The thickness of the walls being small, adequate cross-sectional capacity is usually achieved by folding the metal sheets to form local, internal or end (lips), stiffeners. The behaviour of CFS members is largely governed by their elastic buckling capacity, and it is not unusual that two or more buckling modes interact. In general, local, global, and distortional buckling modes can interact and the governing buckling mode is greatly dependent on the local (cross-section) and global (member) slenderness.

By grouping single members into a composite unit using various types of fasteners, such as screws, bolts and spot welds, structural members with higher axial or bending resistance can be fabricated. These members are referred to as built-up sections and their main advantage is to be characterised by high(er) capacity with reduced weight. Built-up CFS members represent the next generation of structural elements, bringing innovative and efficient new solutions to medium span structures. If these structures are in an aggressive environment, corrosion-resistant stainless steel may be beneficially used [1].

The main challenge in the design of built-up members is to quantify and account for the effect of partial composite action: the inevitable loss in stiffness attributed to longitudinal shear deformations occurring between the individual components, for most types of fasteners, and the resulting development of shear forces in the fasteners is what differentiates built-up sections from solid ones. The loss of flexural rigidity can be brought to a minimum by proper spacing and grouping of fasteners, whose primary role is to maintain the integrity of built-up members undergoing global deformations, such as bending or twisting, induced by buckling. The ability of composite sections to avoid separation and individual (independent) deformations depends on the fastener shear and bearing stiffness, the fastener spacing, the axial stiffness of the individual components and the in-plane stiffness of their connected (contact) areas.

The modified slenderness ratio approach, developed by Bleich [2], is stipulated in most design codes for built-up columns, to account for the lack of full composite action caused by shear deformations at the connection points. The modified slenderness ratio, only applied to the buckling axis requiring fasteners to transfer shear, includes the global slenderness ratio of the built-up section assuming full composite action and the slenderness of individual components between fastener planes. The second term captures the shear deformation associated with the lack of full composite action between the individual components.

Research that has been conducted on cold-formed carbon steel built-up structural elements thus far has provided powerful insight into their stability. These investigations serve as a basis for an in-depth understanding of the behaviour of the equivalent built-up sections made of stainless steel. Rasmussen et al. [3] theoretically showed the influence of partial composite action on the ultimate capacity of CFS built-up members under flexure, torsion, and flexural buckling (FB), with the emphasis on the end-support conditions and longitudinal shear deformations between the individual members. The enhancement in FB strength produced by restraining these deformations can be achieved by grouping the fasteners at the ends, or by using stiff endplates connecting the individual sections. Rasmussen et al. derived expressions for the effective flexural, warping, and torsional rigidities to predict the flexural and torsional deformations of built-up sections as well as their elastic FB loads.

Phan et al. [4] examined the behaviour of CFS lipped channel sections assembled into singly and doubly symmetric cross-sections with a sheet thickness of 1 mm. The members' lengths varied from 500 mm to 6000 mm, covering a broad

spectrum of slenderness, with varying spacing between the fasteners, from 100 mm to 1000 mm, and studied the effects of grouping fasteners at the ends. Interaction of local and distortional buckling happened in all the specimens, with local buckling usually being more dominant for low to intermediate slenderness. With the increase in slenderness, global buckling modes became more pronounced – flexural-torsional for mono-symmetric and FB for doubly-symmetric cross-sections. An interesting observation is that local buckling occurred even for high global slenderness, which was ultimately attributed to the increased local compressive stresses induced by global buckling. Moreover, the use of more rows of fasteners did not significantly improve the overall capacity of built-up members.

In their follow-up research, Phan et al. [5] conducted a finite element parametric study to investigate the effects of different thicknesses, lengths, and fastener spacing on the strength of cold-formed built-up columns. It was demonstrated that the greatest impact of reducing the fastener spacing from 1000 mm to 100 mm was on the strength of the members of intermediate lengths. Moreover, the greatest improvement was for the mono-symmetric specimens, as they undergo torsional deformations during global buckling, therefore their integrity is more impactful to the ultimate strength. However, the general conclusion is that the use of more fastener rows does not substantially increase the capacity of the members.

Becque and Rasmussen [6] investigated the interaction of local and overall flexural buckling in stainless steel I-columns composed of cold-formed back-to-back plain channels, connected with sheet metal screws. Meza et al. [7] performed a comprehensive experimental campaign to examine the structural response and cross-sectional capacity of cold-formed steel built-up stub columns, fabricated from individual channels and flat plates and assembled with bolts or self-drilling screws. In [8], Meza et al. examined the behaviour of 24 pin-ended CFS built-up columns, including four different cross-sectional geometries under compression load with nominal eccentricities of L/1000 or L/1500. The failure of most specimens was governed by the interaction between cross-section instability of the components and global FB of the built-up column, but for some specimens, global buckling of the individual components between fasteners was also observed.

Fratamico et al. [9] conducted an extensive study involving 16 double channel back-to-back cold-formed sections, of length L=1830 mm, with varying cross-sectional properties, with two different web fastener layouts, examining the effects of the fastener layout and end fastener groups on the development of composite action in columns subjected to FB. Fasteners grouped at the end substantially improved the capacity of members with greater sheet thickness, for which global buckling governed the behaviour. For the cross-sections with higher local slenderness where the behaviour is governed by local buckling, grouping of fasteners at the ends did not lead to a significant increase in capacity, which is logical, as the integrity of built-up sections, enhanced by the end fastener groups, is of importance only when the global deformations are prevalent. Therefore, the level of composite action between individual members achieved by fasteners is not shown to have an impact on the increase of local and distortional buckling capacity [10].

Li and Young [11] conducted experiments on 22 pin-ended specimens of lengths 300, 600, 900, 1200, and 1500 mm, with two nominal plate thicknesses of 0.75 mm and 1.2 mm, comprised of folded flange cold-formed channels connected to form open and closed cross-sections. The results for the open cross-sections with sheet thickness of 0.75 mm show the prevalence of local (300 mm) and the interaction of local and distortional buckling (600 mm). FB was observed in more slender specimens. For 900 and 1500 mm, the interaction between distortional and FB was observed, while the 1200 mm long specimen failed by the interaction of local, distortional, and global buckling. For open cross-sections with sheet thickness of 1.2 mm, the 300 and 600 mm long specimens failed by distortional buckling, while the 900, 1200, and 1500

mm long specimens failed through the interaction of distortional and FB. For the closed cross-sections, the interaction of local and distortional buckling was observed for all the specimens, with FB observed for lengths 900, 1200, and 1500 mm.

Selvaraj and Madhavan [12] studied interactive modes of failure in cold-formed doubly-symmetric locally slender back-to-back channel sections. From the total of 41 fixed-ended columns, all but one failed by the interaction of local and global buckling. But what is more interesting is the incidence of the interaction of local and flexural-torsional buckling (FTB) in doubly-symmetric built-up members. This is a consequence of the unsymmetrical local buckling mode imposing redistribution of the compressive stresses, thus altering the effective sectional properties, leading to global torsional deformations − an example of global instability induced by local buckling. The authors showed that, by increasing the spacing between fasteners, the probability of interaction of local and global buckling of an individual member also increases.

EN 1993-1-4 [13] provides supplementary rules, beyond those set out in EN 1993-1-1 [14] for carbon steel, for the design of stainless steel structures. Section 6.4, EN 1993-1-1 [14] prescribes a distinguishable procedure primarily intended for uniform battened or laced built-up columns with pin-ended boundary conditions. The procedure replaces the discrete structure of a built-up column with an equivalent continuous column considering second-order theory and smearing shear stiffness. To restrict the influence of shear deformations between the connected components, it is required that the number of intermediate fastener groups along the column length is not smaller than 2. The rules for closely spaced built-up members are also provided: if the conditions given in Table 6.9 of EN 1993-1-1 [14], related to the maximum spacing between interconnections, are met, the closely spaced built-up member may be designed as a single member by ignoring shear deformations; otherwise, the provisions for battened members should be applied.

The new ANSI/AISC 370-21 Specification [15] for stainless steel structures closely mirrors ANSI/AISC 360-16 Specification [16], but deviate where necessary to account for material nonlinearity and specific features of stainless steel that cause differences in their structural behaviour. Section E.6, ANSI/AISC 370-21 [15], which can be applied to singly and doubly symmetric built-up members composed of two components, provides simplified equations for the modified slenderness ratio depending on the fastener type: snug-tight bolts, and welds or pretensioned bolts. There are also requirements that the end connections of built-up columns must be constructed by means of welds or preloaded bolts. If the ends of the built-up column are connected by welds, the weld length should not be less than the maximum dimension of the built-up cross-section; if the ends of the built-up column are connected by bolts, their mutual longitudinal spacing should not be larger than four times the bolt diameter at a distance that is equal to 1.5 times the maximum dimension of the built-up cross-section. ANSI/AISC 370-21 [15] requires that the slenderness ratio of each individual component should not exceed 75% of the governing slenderness ratio of the built-up member.

Section I1.2 of the North American AISI-S100-16 Specification [18] also entails the modified slenderness ratio approach to determine the FB capacity of built-up columns composed of two components. In order to enforce the condition that buckling of individual components between fasteners does not occur before overall buckling of the built-up column, the following should be fulfilled: (i) the slenderness ratio of the individual component between fasteners cannot exceed 50% of the governing slenderness ratio of the built-up member; (ii) if the ends of the built-up column are welded, the weld length should not be less than the maximum width of the cross-section; also, if the ends of the built-up column are connected by connectors, they should be spaced longitudinally no more than 4 diameters apart for a distance equal to 1.5 times the maximum width of the cross-section; and (iii) the intermediate connections designed by fasteners or by welds should be

capable of transmitting the load in any direction equal to 2.5% of the nominal compression resistance of the built-up member. The modified slenderness ratio method cannot predict the effects of fastener spacings on torsional, flexural-torsional, local, or distortional buckling modes.

The insufficient clarity of the codified design procedures related to torsional and flexural-torsional ultimate responses is the main motivation for this paper. The paper describes a nonlinear finite element model (FEM) used to study pin-ended cold-formed stainless steel (CFSS) built-up columns comprising (i) two equal-leg angle components, oriented back-to-back to form a T-section and (ii) four equal-leg angle components, star-oriented to form a cruciform cross-section. A characteristic of the considered cross-sections is that their walls' mid-lines intersect at a single point and that their primary warping resistance is minute. This implies extremely low torsional stiffness, which makes these columns highly susceptible to buckling phenomena involving torsion i.e, torsional buckling (TB) or FTB. The finite element (FE) models are calibrated and validated against the results of (i) two repeated tests on short-length CFSS built-up T-section columns composed of two back-to-back equal-leg angles made of lean-duplex grade EN 1.4162, and (ii) four repeated tests on short- and medium-length CFSS built-up cruciform-section columns composed of four star-oriented equal-leg angles made of austenitic grade EN 1.4162, firstly presented herein. A parametric study is subsequently performed to obtain the ultimate buckling resistances for a wide range of cross-section slenderness values and column lengths considering different stainless steel families (austenitic, duplex, and ferritic). The FE results are employed to assess the applicability of the current Direct Strength Method (DSM) stated in AISI-S100-16 [18] for the studied built-up sections, including the recently proposed design procedure for built-up sections comprising 3 or more components and failing in global flexural or FTB modes [3], [4], [5]. Comparisons between the numerical results are also made against the provisions for the design of built-up columns stated in EN 1993-1-4 [13], 1993-1-1 [14], and AISC 370 [15]. The reliability of the considered design procedures is demonstrated through statistical analyses.

2 Experiment

2.1 Test design and preparation

The experiments were conducted at the University of Belgrade, Faculty of Civil Engineering, and are part of a scientific investigation primarily addressing single cold-formed, hot-rolled and laser-welded stainless steel equal-leg angle columns with pin-ended boundary conditions [19], [20], [21]. The experimental campaign included 6 global buckling tests on built-up specimens under pure axial compression. The built-up T-section specimens were composed of two back-to-back CFSS equal-leg plain angle sections with nominal dimensions of 80 × 4 mm and an internal corner radius of 12 mm. The built-up cruciform-section specimens were composed of four star-oriented CFSS equal-leg plain angle sections with nominal dimensions of 60 × 3 mm and an internal corner radius of 6.5 mm. Both angle-sections are classified as Class 4, according to the slenderness limits prescribed in EN 1993-1-4 [13]; their nominal geometric properties are shown in Table 1. The components (angle-section) that made up the T-section specimens were produced from hot-rolled sheet made of lean-duplex stainless steel grade EN 1.4162 (UNS S32101), X2CrMnNiN21-5-1, having nominal yield stress of 480 MPa [22]. The components that made up the cruciform-specimens were produced from a cold-rolled sheet made of austenitic stainless steel grade EN 1.4301 (UNS S30400), X5CrNi18-10 with a nominal yield stress of 230 MPa [22]. Considering pin-ended (simple-simple) boundary conditions for a nominal equal-leg angle section under compression, in the computer program CUFSM [23], the elastic flexural-torsional buckling stress and the corresponding half-wavelength were found to be respectively 187.2 N/mm^2 and 1500 mm for angle 80 × 4 mm, and 186.5 N/mm^2 and 1100 mm for angle 60 × 3 mm (FTB mode of short length angle column features a deformed shape similar to that of local buckling). This analysis served as a guideline for choosing the specimen length for the built-up specimens. A nominal length of 1000 mm was adopted for the

built-up T-section specimens, whereas nominal lengths of 600 mm and 2400 mm were adopted for the built-up cruciform-section specimens to ensure failure modes FTB and TB respectively. Taking into account the above data from the CUFSM program [23], to avoid FB of cruciform-section columns it was decided to test the built-up cruciform-section specimens under fixed-ended boundary conditions. Two repeated tests were included for each specimen length.

Table 1 Nominal geometry of the single angle sections.

Angle section	A (mm^2)	I_y (mm^4)	I_z (mm^4)	I_u (mm^4)	I_v (mm^4)	J (mm^6)	I_w (mm^6)
∟80 × 4	599.4	383460.7	383460.7	632113.7	134807.6	3196.8	196650.6
∟60 × 3	340.5	122378.2	122378.2	200114.5	44641.9	1021.4	13447.5

The component sections were connected by discrete fasteners. The fasteners are M8 bolts, class 8.8, with nominal yield strength f_{yb} = 640 N/mm^2 and ultimate tensile strength f_{ub} = 800 N/mm^2. The hole diameter in the angle legs was 9 mm and a 1 mm bolt-to-hole clearance was provided. The bolted connection corresponds to the shear connection category A, EN 1993-1-8 [24]. The end fastener group (EFG) had a length equal to the maximum dimension of the built-up angle section 2*b* (120 mm and 160 mm for angles 60 × 3 mm and 80 × 4 mm, respectively) and exhibited bolt spacing of 40 mm (i.e. approximately four bolt diameters apart). The EFG was utilised to minimise the relative slip between the components, which could potentially improve the global buckling resistance of the columns. The specimens also had intermediate fastener groups (IFGs) evenly spaced along the member, as shown in Fig. 1. The principal axes of the singly-symmetric equal-leg T-section are the geometric axes, the *y*-*y* axis is the minor principal axis, whereas the *z*-*z* axis is the major principal axis lying in the built-up section buckling plane. In the case of doubly-symmetric equal-leg cruciform-sections every centroidal axis can be considered as the principal axis (the axes *u*-*u* and *v*-*v* are at 45° to the geometric axes *y*-*y* and *z*-*z*, both lying in the built-up section buckling plane).

The labelling convention for the test specimens is "⊤(÷) *b* × *t* × *L* – *a* – *m* – *X*", where the first symbol "⊤" or "÷" indicates the shape of the built-up cross-section, followed by the nominal section sizes in millimetres (leg width *b* × thickness *t*), "*L*" is the length of the FE column, "*a*" is the centre-to-centre distance between two adjacent fastener connections, "*m*" is the number of centre-to-centre distance between two adjacent fastener connections, and "*X*" is the a sequential number which relates to the repeated specimens.

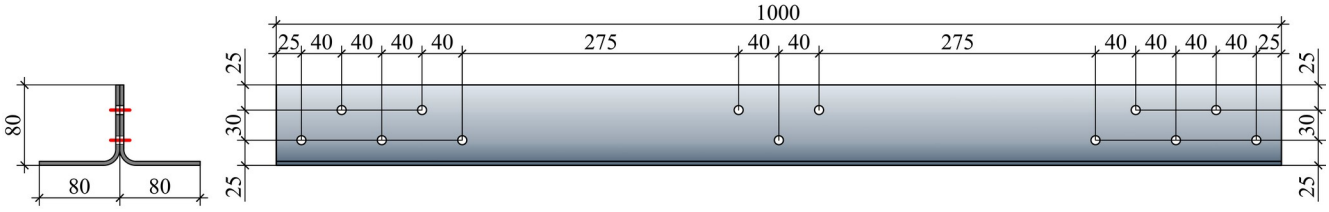

(*a*) Built-up T-section specimens ⊤ 80 × 4 – 1000 – 395 – 2

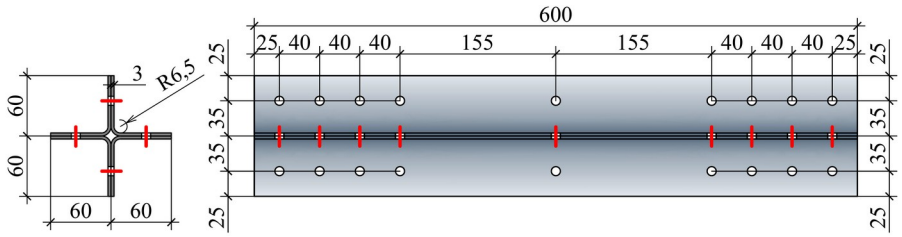

(*b*) Built-up cruciform-section specimens ÷ 60 × 3 – 600 – 235 – 2

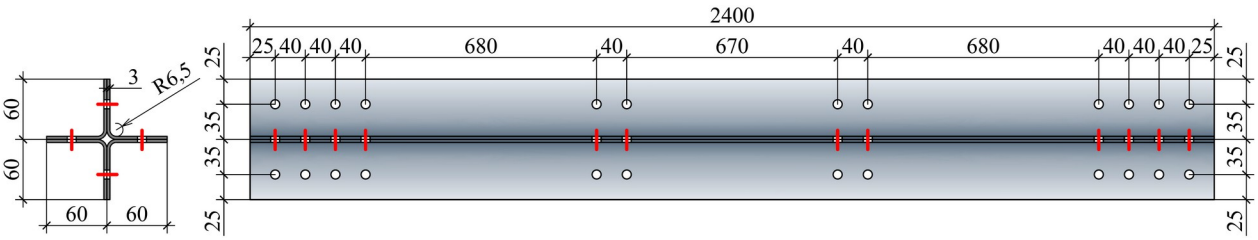

(*c*) Built-up cruciform-section specimens ÷ 60 × 3 – 2400 – 780 – 3

Fig. 1 Geometric parameters of built-up specimens (all dimensions are in mm).

To obtain mechanical material properties of tested columns, tensile tests were performed on flat and corner coupons extracted from the final press-braked sections under strain-control according to the requirements of EN ISO 6892-1 [25]. The tests were carried out on an AG-Xplus Universal Testing Machine (Shimadzu, Japan) with a capacity of 300 kN. Average values of key mechanical properties are summarized in Table 2, in which E is the modulus of elasticity, f_y is yield strength taken as the 0.2% proof stress, $\sigma_{0.01}$, $\sigma_{0.05}$, $\sigma_{1.0}$ are different proof stresses, f_u is the ultimate tensile strength, ε_u is the strain corresponding to the ultimate tensile strength, ε_f is the total strain at fracture, and n and m are the strain hardening parameters utilised in the Ramberg–Osgood material model for nonlinear metallic materials [26].

Table 2 Average measured material properties of the tested specimens obtained from tensile coupon tests.

Stainless steel grade / Angle-section	Coupon	f_y (N/mm^2)	$\sigma_{0.01}$ (N/mm^2)	$\sigma_{0.05}$ (N/mm^2)	$\sigma_{1.0}$ (N/mm^2)	f_u (N/mm^2)	E (N/mm^2)	ε_u (%)	ε_f (%)	Strain hardening parameters	
										n	m
EN 1.4162 **[19]** / ∟80 × 4 mm	Flat leg coupons	517	350	424	588	768	197445	31	45	7.9	3.0
	Corner coupons	703	586	641	788	823	199905	17	33	11.0	13.1
EN 1.4301 / ∟60 × 3 mm	Flat leg coupons	310	198	251	349	640	201103	50	56	8.1	2.2
	Corner coupons	458	246	345	511	680	194440	36	45	5.0	2.5

The shear properties (the load-displacement curves and measured shear stiffness) of the bolt connections were obtained from two repeated single lap shear tests. The connection plates of each specimen were fabricated from cold-rolled sheet with thickness of 3 mm, made of austenitic stainless steel grade EN 1.4301, and assembled with two bolts aligned with the tensile load. Nominal clearances of 1mm for M8 bolts, class 8.8 were used. The end distances and the spacing between bolts, in the load direction, were respectively 40 mm and 80 mm whereas the edge distance of the bolt row was 40 mm; these data were chosen in accordance with the recommendations in ECCS TC7 [27]. The plates were connected by hand bolt tightening. The steel plates had a nominal width of 80 mm, which was reduced to 50 mm at the ends to adjust the specimen into the grips of the testing machine. The tests were carried out on an AG-Xplus Universal Testing Machine (Shimadzu, Japan) with a capacity of 300 kN. The adopted strain rates were 0.5 mm/min. Two linear variable displacement transducers (LVDTs) were set-up to measure the elongation of the connection part over 190 mm. The load-elongation curves were obtained by averaging the deformations recorded by both LVDTs. A schematic view of the single lap bolted connection test is shown in Fig. 2a, whereas the average load-elongation curves are shown in Fig. 2b. The labelling convention of the specimens is “BC (Bolt Connection) – bolt diameter – specimen number”.

(*a*) Single lap shear test set-up

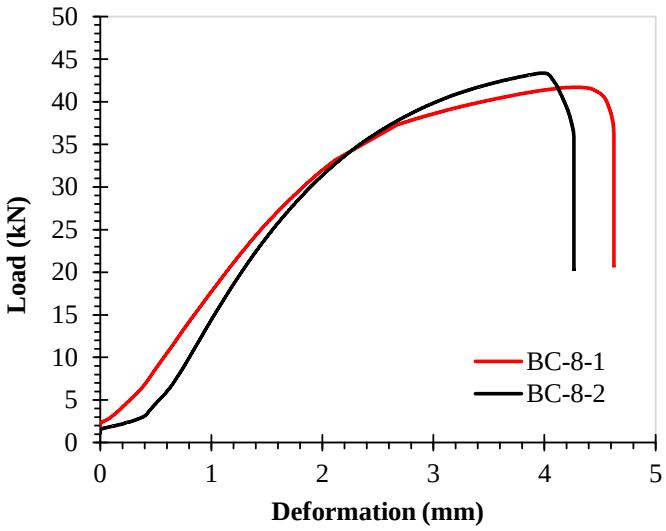

(*b*) Average load-elongation graphs obtained for the single shear tests

Fig. 2 Single lap shear bolt connection test.

The initial geometric imperfections of the specimens were measured before testing, using a multiplanar portable laser tracker Leica Absolute Tracker AT960 (Hexagon Manufacturing Intelligence, UK). With optical centring accuracy of +/-3 µm, the method offers highly accurate results within 15 + 6 µm/m for line-of-sight measurements. A more detailed description can be found in [19], [20], [21], while only a brief summary is provided herein. Full-field geometric data of the specimen was expressed as a point-grid by measuring the outer surfaces of the specimen and registering the individual set of measurements into the same final global coordinate system. The point-grids therefore consist of nodal points measured for a set of cross-sections along the specimen's length. The imperfection distribution and amplitudes are obtained from the reconstructed three-dimensional point-grids acquired by the laser tracker. As shown in Fig. 3, four types of geometric imperfections were measured: local imperfections ω related to cross-sectional distortion and 3 global imperfections: bow imperfections δ_y perpendicular to the *y*-*y* axis, camber imperfections δ_z perpendicular to the *z*-*z* axis and twist imperfections θ. Fig. 3 also shows the sign convention employed when measuring the global imperfections: a positive sign of bow and camber imperfections is in correspondence with the *y* and *z* axes, whereas the twist imperfection measurements are positive clockwise. The imperfection data are summarised in Table 3.

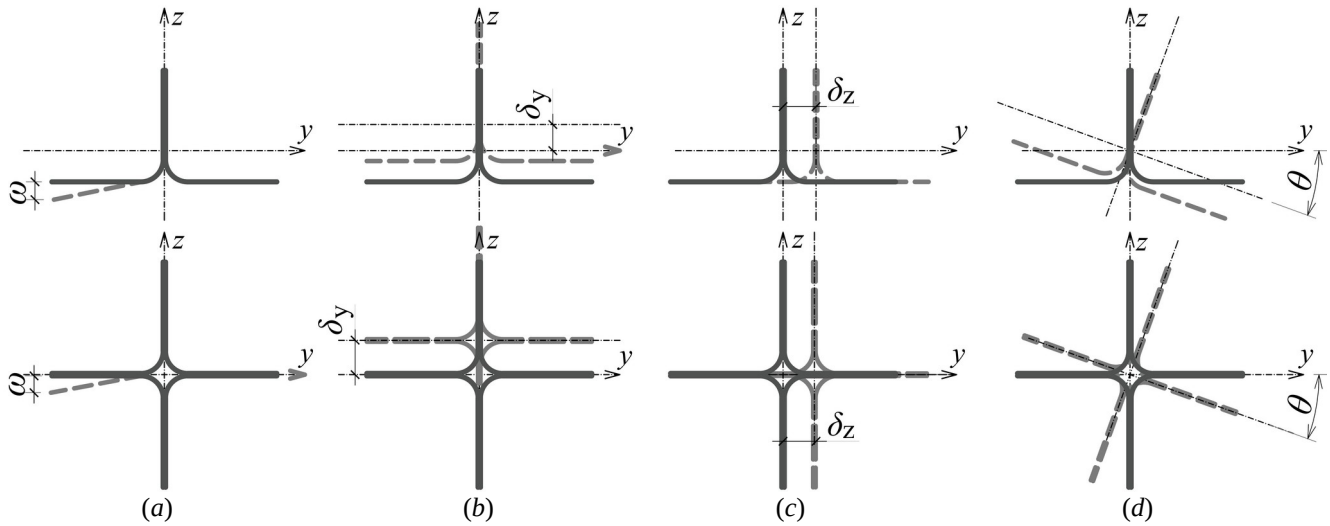

Fig. 3 Measured imperfections: (*a*) cross-section imperfection; (*b*) bow imperfection; (*c*) camber imperfection; (*d*) twist imperfection.

Table 3 Maximum measured initial geometric imperfections.

Specimens	ω_0 (mm)	ω_0/b (-)	$\delta_{0,y}$ (mm)	$\delta_{0,y}/L$ (-)	$\delta_{0,z}$ (mm)	$\delta_{0,z}/L$ (-)	θ_0 (º)	θ_0/L (º/m)
⊤ 80 × 4 – 1000 – 395 – 1	0.128	*b*/625	-0.189	*L*/5291	-0.115	*L*/8696	0.150	0.150
⊤ 80 × 4 – 1000 – 395 – 2	0.221	*b*/362	0.105	*L*/9523	-0.255	*L*/3921	0.197	0.197
÷ 60 × 3 – 600 – 235 – 1	0.068	*b*/882	0.451	*L*/1330	0.310	*L*/1935	0.258	0.258
÷ 60 × 3 – 600 – 235 – 2	-0.125	*b*/480	0.290	*L*/2069	0.411	*L*/1460	0.410	0.410
÷ 60 × 3 – 2400 – 780 – 1	-0.090	*b*/667	-1.014	*L*/2367	-0.910	*L*/2637	0.158	0.158
÷ 60 × 3 – 2400 – 780 – 2	0.158	*b*/380	0.801	*L*/2996	-0.704	*L*/3409	-0.410	-0.410

The buckling tests were carried out at the Laboratory for testing of structures at the Institute for testing of materials in Belgrade, Serbia in a hydraulic testing machine (Amsler, Switzerland) with a maximum capacity of 2000 kN. The used testing procedure is consistent with that reported in [19]. The axial load was measured via a 200 kN load cell C6A Force Transducer (HBM, Germany) installed at the bottom loading plate. Loading was displacement-controlled with a load rate not exceeding 0.01 mm/s.

Fig. 4 shows the setup used for the tests on the built-up T-section columns. Lateral bi-planar displacements and overall rotation of the built-up cross-section were tracked throughout the tests using 12 LVDTs, placed on each leg of the angle section: 4 were mounted at mid-height (see Fig. 4, section BB) and 4 more were placed at a distance of 200 mm from each specimen ends (see Fig. 4, sections AA and CC). Lastly, considering that the specimen undergoes major axis FTB, "shear slip" LVDTs were installed inside the EFGs [28], to monitor the relative slip of the individual angle legs in contact and quantify the degree of composite action provided by hand-tightened bolted connections (see Fig. 4, section CC). These LVDTs were attached via additional steel plates and did not disrupt the cross-sectional deformation. The instrumentation also consisted of six linear strain gauges (SGs) affixed onto the section at mid-height to determine the axial compressive strains at the extreme fibres of the angle legs (see Fig. 4, section BB). To provide a pinned boundary, hardened knife-edge devices allowing rotations about the minor-axis, while restraining major-axis rotations, as well as twist rotations and warping were used. Steel clamps with slotted holes and bolts were used to enable the specimen to be adjusted in the rig and clamped to the loading plates (preventing detachment between the specimen end cross-sections and the plates), see Fig. 5. These clamps allowed a degree of shear flexibility, ensuring the EFG is effective in shear. The specimen ends were milled flat to ensure full contact with the loading plates. The effective length L_e is defined as the distance between the two hinges

for the pin-ended condition, equal to L plus 2 times 90 mm, where L is the specimen length and 90 mm is the distance from the specimen's end to the respective pin at each end (see Fig. 4).

The built-up cruciform-section specimens were also installed within the sliding steel clamps rested on the loading plates of the test machine (see the test setup shown in Fig. 6). Likewise, these boundary conditions provide partial rotational restraint to the column ends, and do not prevent end shear deformations between the individual components ensuring the key role of the EFG. The instrumentation also consisted of 12 LVDTs: four at mid-height to record torsional displacements (Fig. 6, section AA); four on the bottom plate of the testing machine to measure the vertical movement (i.e., end shortening), see Fig. 6, section EE; four additional "shear slip" LVDTs were placed in the middle of the EFGs (Fig. 6, section CC). For the specimens with short length (600 mm), four more LVDTs were placed halfway between EFG and IFG (Fig. 6, section BB) whereas for the 2400 mm long specimens, the displacements at mid-height were recorded via eight SGs. This cross-section is also halfway between adjacent IFGs, see Fig. 6, section AA.

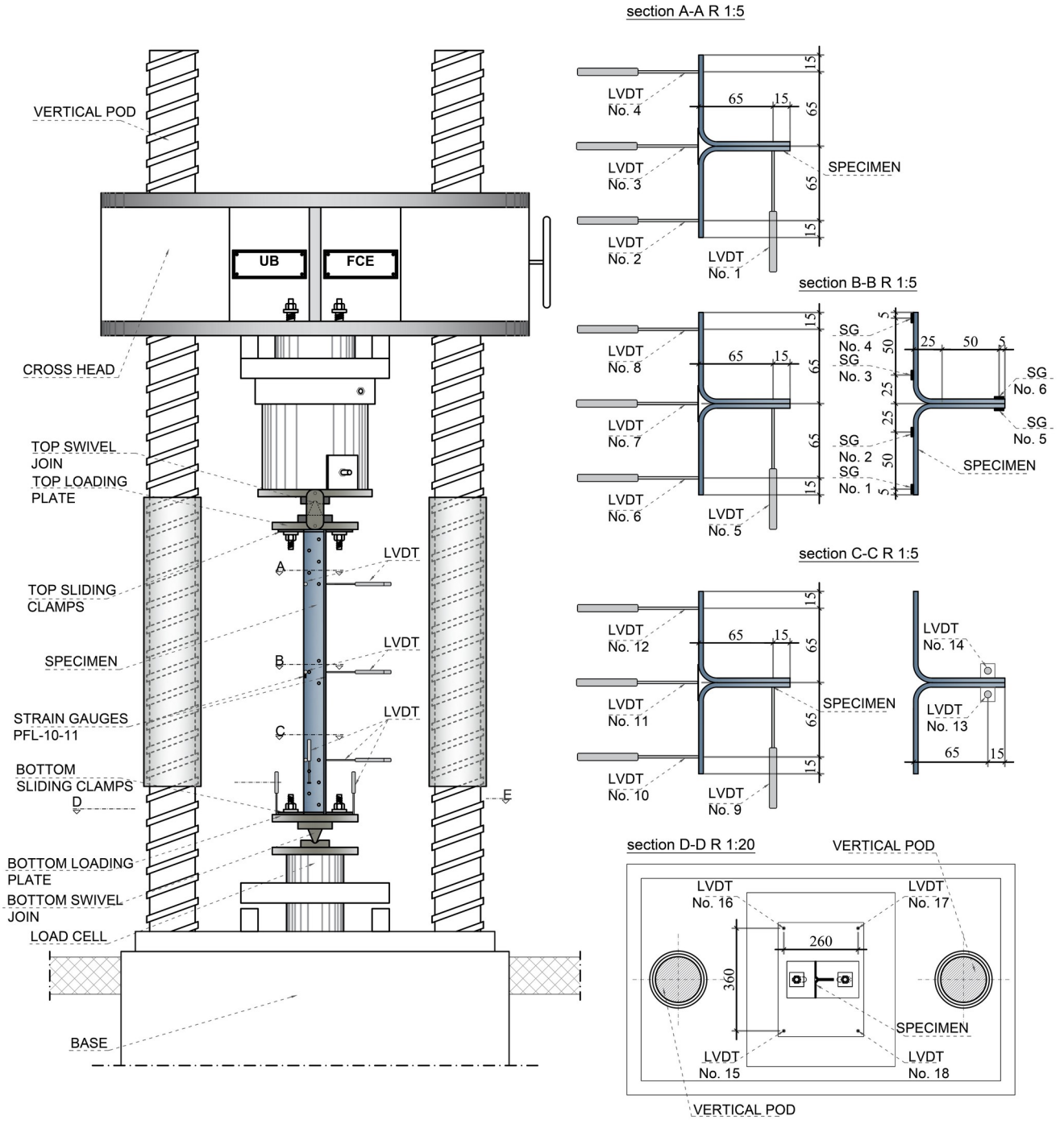

Fig. 4 Test setup and instrumentation configuration for buckling tests on the built-up T-section columns (all dimensions in mm).

1

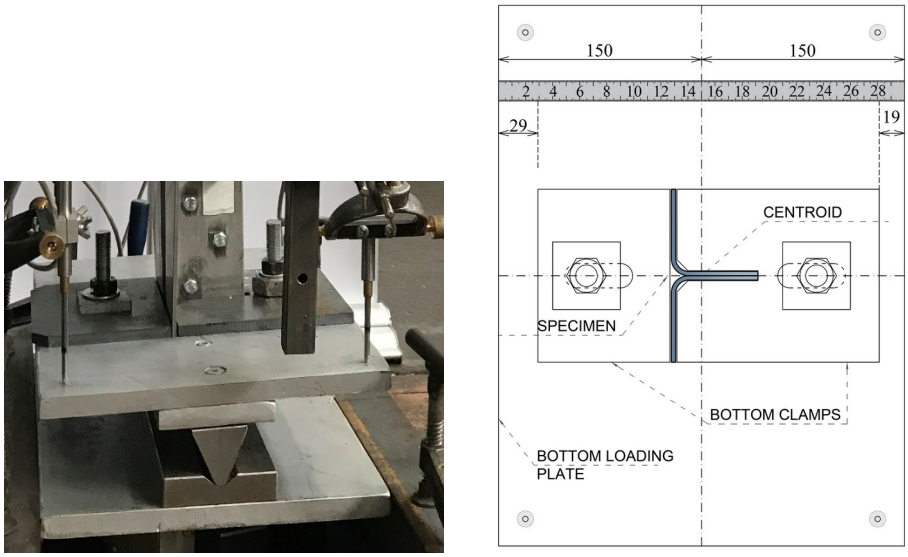

Fig. 5 Boundary condition at the bottom of the built-up T-section column ─ knife-edge devices and steel clamps (all dimensions in mm).

1

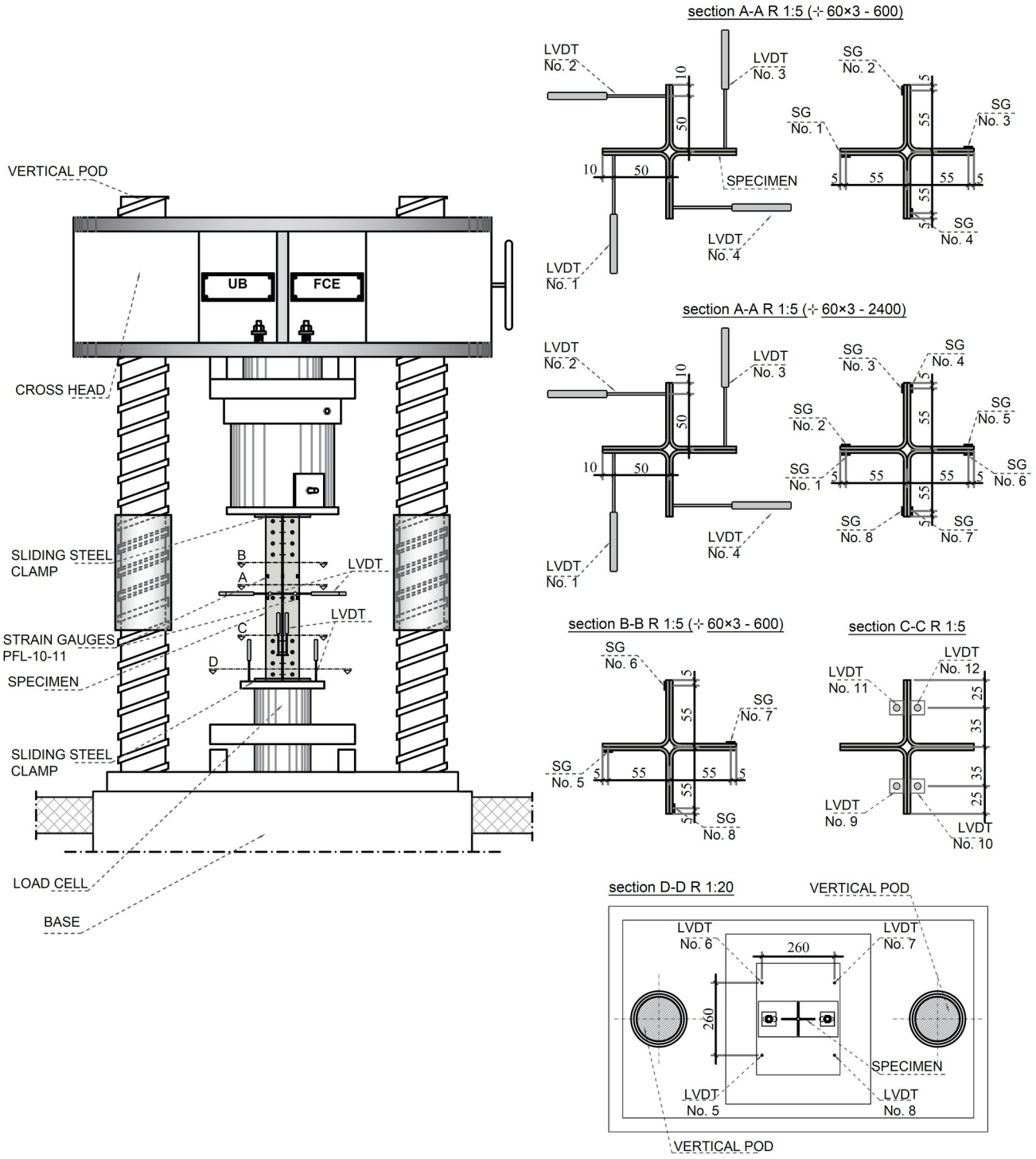

Fig. 6 Test setup and instrumentation configuration for buckling tests on the built-up cruciform-section columns (all dimensions in mm).

2.2 Test results

The deformed shape of the specimens ⊤ 80 × 4 – 1000 – 395 – 1, ⊹ 60 × 3 – 600 – 235 – 1 and ⊹ 60 × 3 – 2400 – 780 – 2 after buckling (at approximately 30% post-peak capacity) is shown in Fig. 7.

The bi-planar lateral deflections and twisting at mid-height of the built-up sections were determined based on readings from the LVDTs, by applying the appropriate mathematical transformations described in the procedure developed by Landesmann et al. [29]. The signs of the mid-height lateral deflections correspond to the *y* and *z* axes convention, whereas the torsional rotations φ are positive clockwise, see Fig. 8a showing an undeformed and deformed configuration of the

considered built-up sections in the *y*–*z* coordinate system. Positive readings of lateral deflections indicate a specimen which moves away from the LVDT initial positions, whereas negative readings are those for which the specimen moves towards the LVDT initial positions, as shown in Fig. 8b.

Key experimental results presented in graphical form as load–torsional displacement and load–axial strain curves are shown in Fig. 9 to Fig. 14, at mid-height for a selection of specimens. The load–relative shear slip between each component curves within the built-up section columns are shown in Fig. 15.

Table 4 provides a summary of all experimental results, in which $P_{b,u,exp}$ is the maximum axial load capacity (failure load), $d_{u,y}$ and $d_{u,z}$ are the mid-height lateral deflections about minor and major principal (and geometric) axes, respectively, and φ_u is the mid-height torsional rotation corresponding to the failure load, with respect to the centroid of the built-up cross-section.

As indicated in Fig. 7a and Table 4, global major-axis FTB was observed as the primary limit state for both built-up T-section columns without any observed localized failure or separation of the areas in contact. For specimen ⊤ 80 × 4 – 1000 – 395 – 1, Fig. 9 shows a uniformly increasing trend followed by significant growth of lateral deflections in both major- and minor-axis directions after the ultimate load is reached. The gradual growth of longitudinal strains, shown in Fig. 10 (⊤ 80 × 4 – 1000 – 395 – 1), demonstrates a uniform application of the compression load at mid-height in the early loading phase. However, in the post-peak load, the nonuniform distribution - with higher compressive strains at one flange end (SG4), lower compressive strains (SG1) at the other flange end and tensile strains in the web (SG5 and SG6) of the built-up T-section - indicate interaction of FTB with minor-axis FB. The shear slip between the bolt-connected angle legs was measured to be 1.43 mm, at the peak-load, see Fig. 15a. This is due to the diameter of the bolt hole being 1 mm larger than that of the bolt, which allows the two component sections to slide relative to each other as the bolts do not come into contact with the bolt hole walls, during loading.

The governing failure mode for short length built-up cruciform-section specimens was TB, as demonstrated in Fig. 11 and Fig. 12 for specimen ÷ 60 × 3 – 600 – 235 – 1, and in Table 4. Almost uniform readings for the lateral displacements of the section legs indicate a pronounced torsional rotation φ at mid-height, whereas the flexural displacements are negligible (the maximum displacements at peak-load are 0.407 mm along *y*-*y* axis and 1.319 mm along *z*-*z* axis). Fig. 11 also reveals high torsional stiffness throughout the entire loading regime. The distribution of the longitudinal strains demonstrates a relatively uniform application of the compression load. The strain (stress) distributions at mid-height (where the individual components are connected) are characterized by a change in sign; at peak load, nonuniform cross-sectional stress distribution occurs and exhibits both compressive and tensile stresses at the leg tips. However, the cross-section leg tips at half the distance between EFG and IFG are predominantly under tensile stresses throughout the loading phase (see Fig. 12). In particular, the slender legs (as outstanding parts of individual leg components) exhibit transverse bending — this is due to smaller rotational restraint stemming from the absence of bolt interconnection, see Fig. 7b. The shear slip between the bolt-connected angle legs was measured to be 1.98 mm, at peak-load, see Fig. 15b. Localized failure or separation of the contact areas were not observed, nor bolt shear failure with increasing load.

The dominant failure mode for longer built-up cruciform-section specimens was TB coupled with global and local lateral deflections, as displayed in Fig. 7c (÷ 60 × 3 – 2400 – 780 – 2) and summarised in Table 4. Localised distortions of individual angle components were not visible before the peak load was reached, nor did bolt shear failure occur. The experimental axial load versus torsional displacements curve (see Fig. 13) indicates that the failure mode involved notable

twisting in combination with FB behaviour; at peak load, the maximum lateral displacements (deflections) measured at mid-height are 1.847 mm along *y-y* axis and 5.957 mm along *z-z* axis. The separation of the ascending branches of the load–displacement response, occurring in the early loading phase, indicates the appearance of transverse bending of the individual angle legs and their sensitivity to local buckling — this is due to the absence of individual component connection at mid-height. Note that the built-up cruciform-section specimens were tested under semi-rigid support conditions with their end cross-sections flush with the plates of the testing machine. In general, when buckling deformations are amplified, the deformed legs can lift-off from the bearing plate, thereby changing the cross-sectional stress distribution and influencing the effectiveness of the EFGs. The longer built-up cruciform-section specimens also exhibited lower torsional rotations φ in comparison with shorter specimens. Therefore, the structural behaviour of slender specimens is also affected both by the experimental boundary conditions at the column ends, and by their susceptibility to the FB.

The observed failure mode is confirmed by the axial strain distribution recorded by the SGs (see Fig. 14). Axial strains at the mid-height are in compression throughout the entire loading regime. The ascending branches of the load–axial strain response gradually separate prior to the peak, as the applied load, lateral and torsional displacements increase. In the post-peak load regime, global buckling was followed by separation of the individual angle components between IFGs. As shown in Fig. 14, tensile strains occur at the leg tips of two adjacent individual components (SG4 – SG7), whereas in the other two individual components, one leg tip was in tension (SG2, SG8) and the other was compressed (SG1, SG3). The shear slip between the angle legs was measured to be 0.83 mm, at peak load, see Fig. 15c. Separations of individual components directly adjacent to EFGs were also observed in the post-peak load regime, which is where shear deformations are significant, see Fig. 7c. The role of EFGs in preventing shear slip was key.

(*a*) ⊤ 80 × 4 – 1000 – 395 – 1 (*b*) ÷ 60 × 3 – 600 – 235 – 1 (*c*) ÷ 60 × 3 – 2400 – 780 – 2

Fig. 7 Failure mode observed at approximately 30% post-peak capacity

1

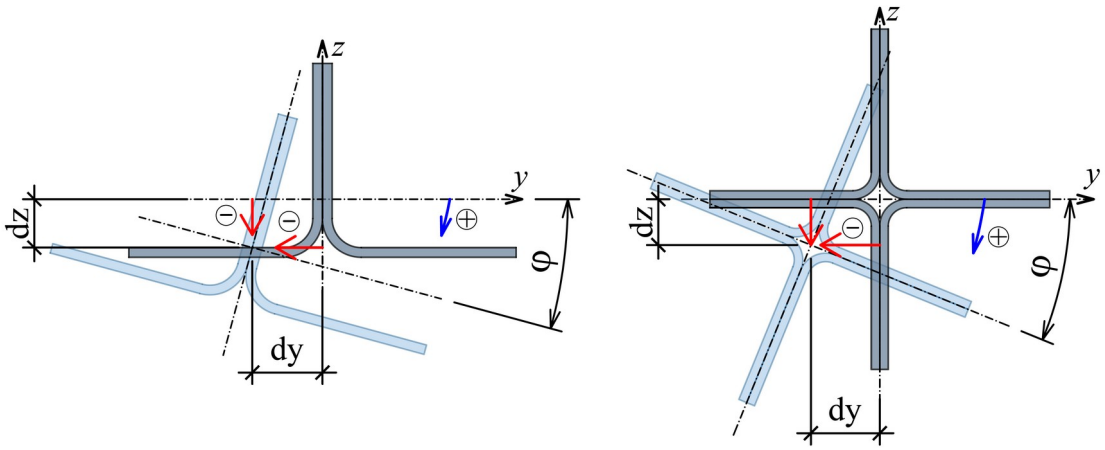

(*a*) Schematic of the sign convention for lateral deflections and torsional rotations with respect to the y–z coordinate system

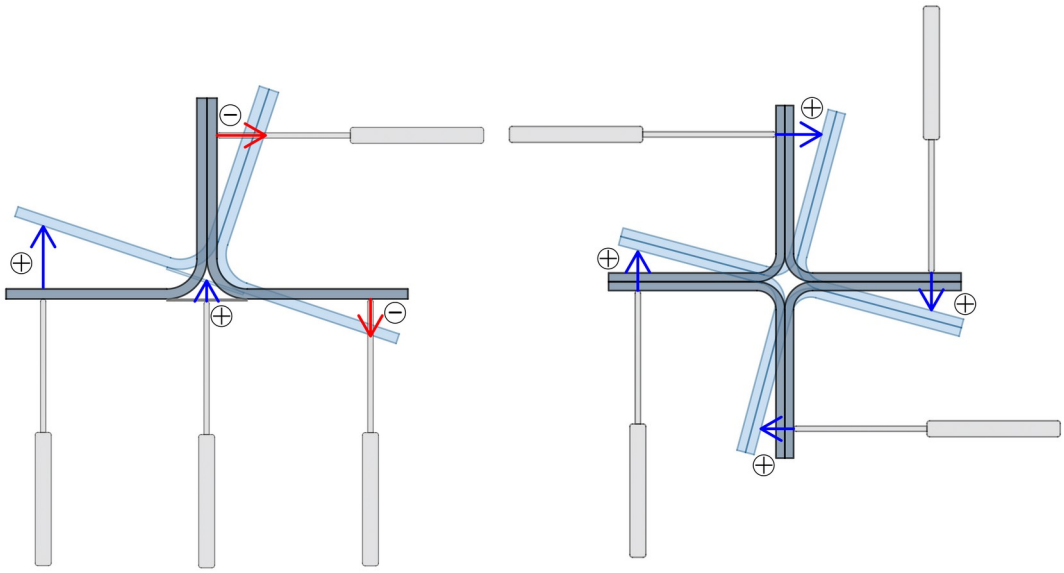

(*b*) Schematic of the sign convention for lateral deflections with respect to the initial LVDT positions

Fig. 8 Undeformed and deformed built-up section configuration.

1

2

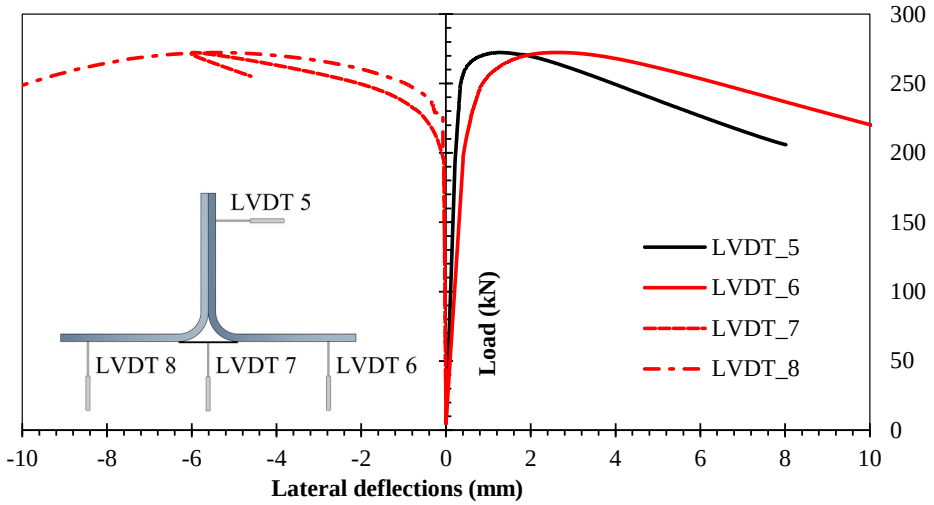

Fig. 9 Load versus lateral deflection curves at mid-height of the specimen ⊤ 80 × 4 – 1000 – 395 – 1.

3

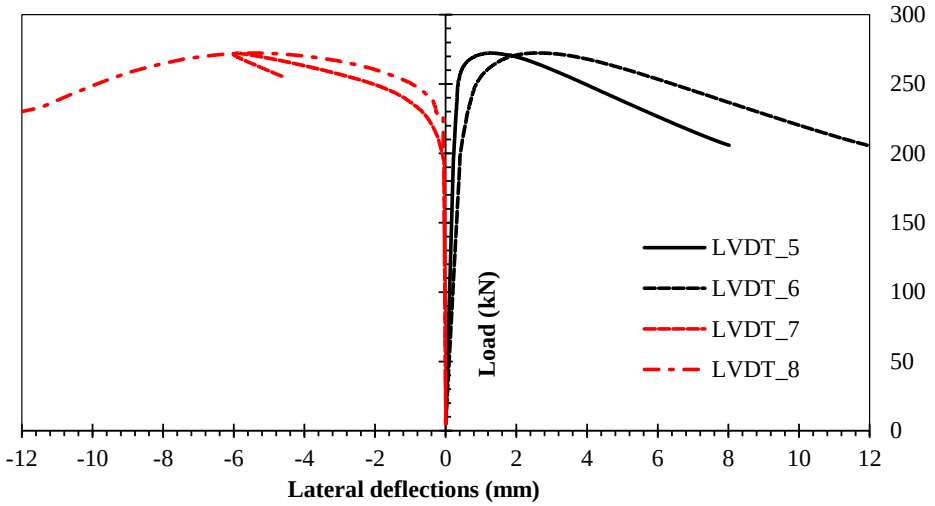

Fig. 10 Load versus axial strain curves at mid-height of thespecimen ⊤ 80 × 4 – 1000 – 395 – 1.

1

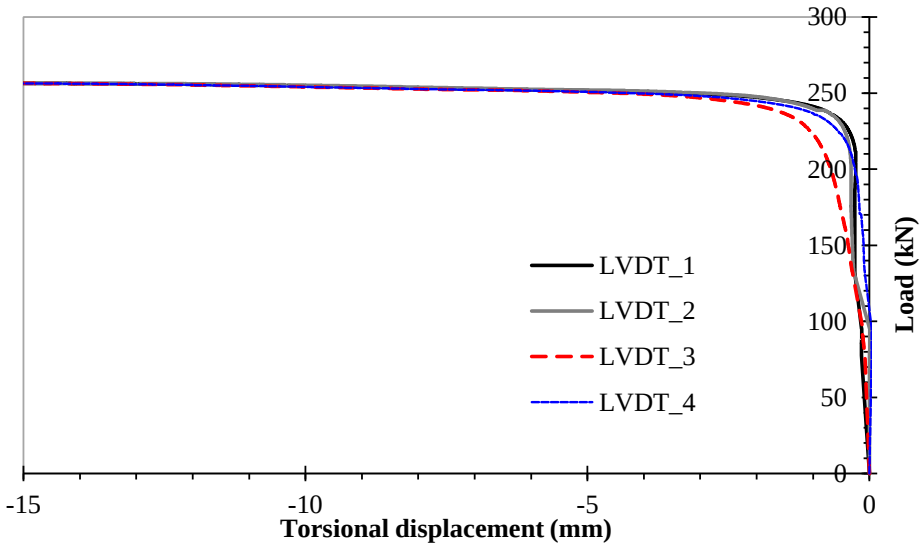

Fig. 11 Load versus torsional displacement curves at mid-height of the specimen ÷ 60 × 3 – 600 – 235 – 1.

2

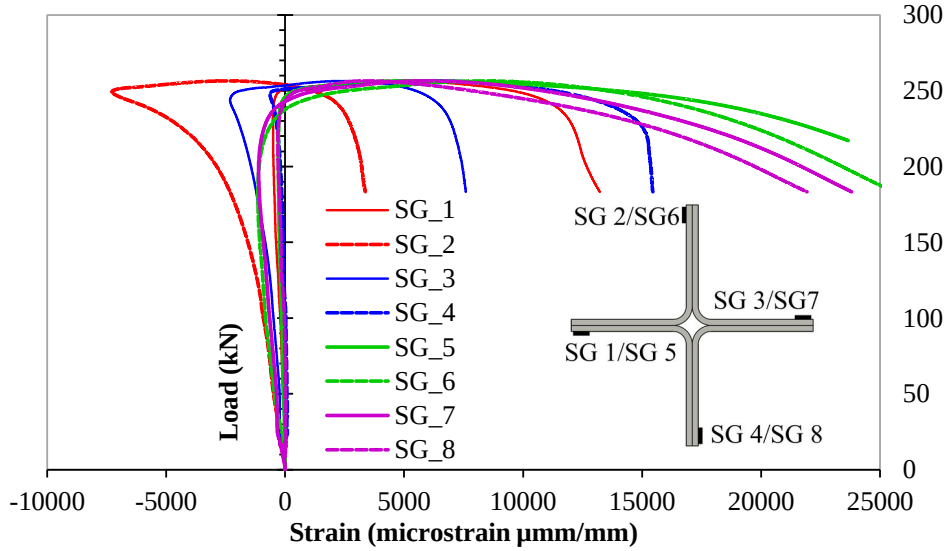

Fig. 12 Load versus axial strain curves at mid-height of the specimen ÷ 60 × 3 – 600 – 235 – 1.

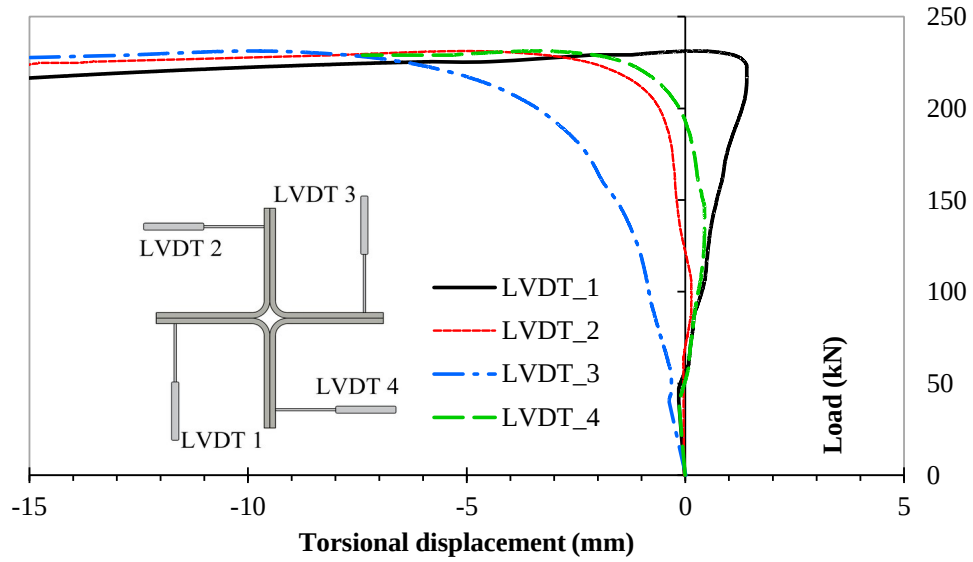

Fig. 13 Load versus torsional displacement curves at mid-height of the specimen ÷ 60 × 3 – 2400 – 780 – 2.

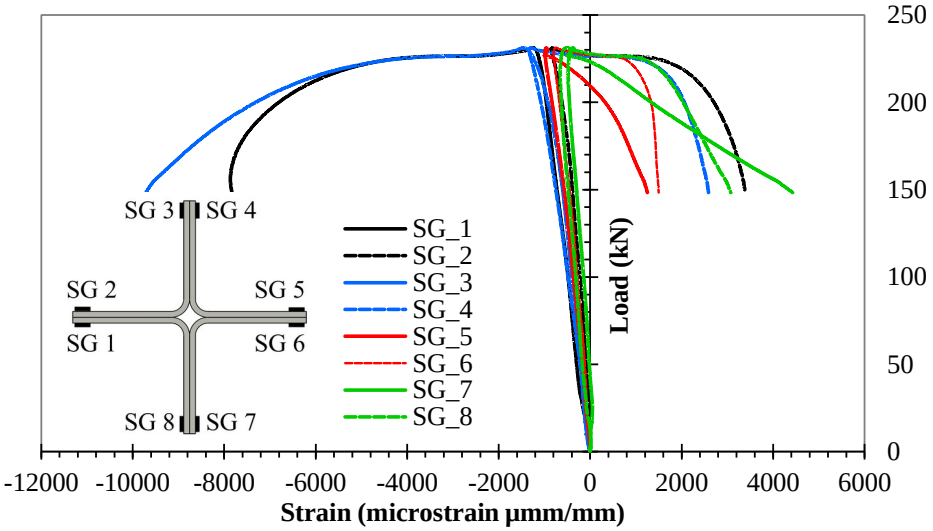

Fig. 14 Load versus axial strain curves at mid-height of the specimen ÷ 60 × 3 – 2400 – 780 – 2.

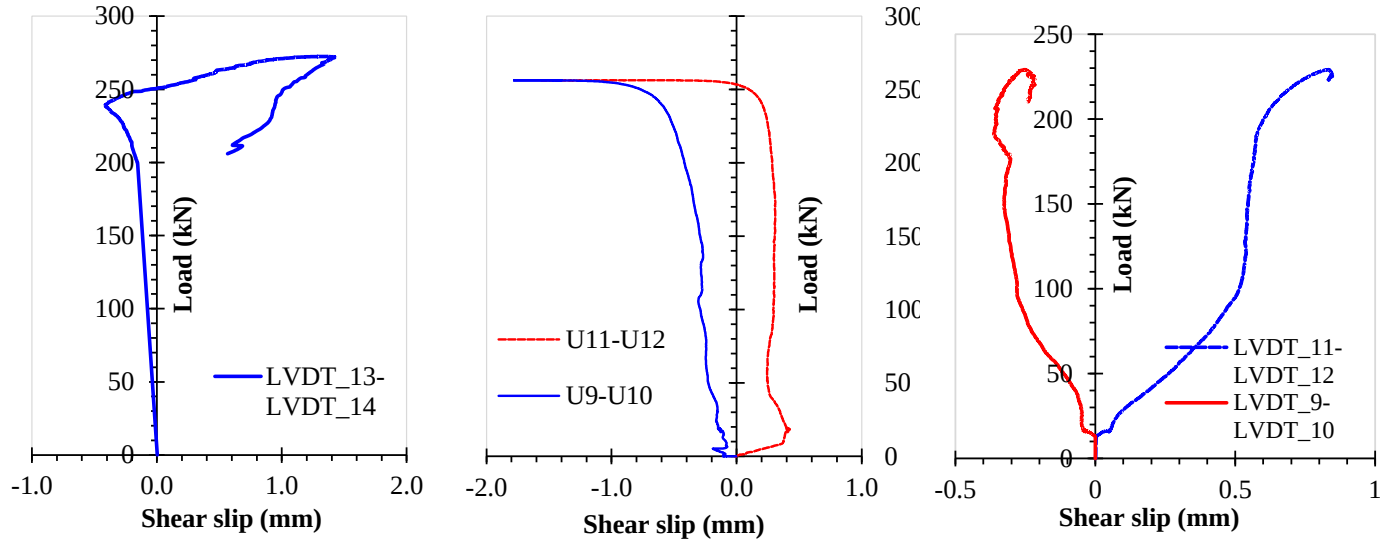

(*a*) ⊤ 80 × 4 – 1000 – 395 – 1 (*b*) ÷ 60 × 3 – 600 – 235 – 1 (*c*) ÷ 60 × 3 – 2400 – 780 – 2

Fig. 15 Load versus shear slip curve showing the amount of slip between the bolted legs.

Table 4 Summary of buckling test results.

Specimens	Governing failure mode	$P_{b,u,exp}$ (kN)	$d_{u,y}$ (mm)	$d_{u,z}$ (mm)	φ_u (deg)
⊤ 80 × 4 – 1000 – 395 – 1	FTB	272.4	+1.443	–1.337	+3.538
⊤ 80 × 4 – 1000 – 395 – 2	FTB	283.2	+16.444	–8.392	+9.469
÷ 60 × 3 – 600 – 235 – 1	TB	265.2	+0.407	+1.319	+12.577
÷ 60 × 3 – 600 – 235 – 2	TB	256.4	+0.926	+0.492	-16.816
÷ 60 × 3 – 2400 – 780 – 1	TB	231.3	-1.318	+6.230	-8.307
÷ 60 × 3 – 2400 – 780 – 2	TB	229.2	+1.847	+5.957	-7.629

3 Numerical study

The commercial software ABAQUS [30] was used to create FE models aiming at replicating the buckling tests on built-up specimens presented in Section 2. Validation of the FE models against the generated experimental data on CFSS built-up columns is first presented. The pin-ended built-up T-section columns comprising two back-to-back equal-leg angles, and built-up cruciform-section columns comprising four star-oriented equal-leg angles under semi-rigid boundary conditions, were considered in the model validation to demonstrate the applicability of the developed models.

In Section 3.2, a parametric study is conducted to investigate the behaviour of CFSS built-up T- and cruciform-section columns made of different stainless steel grades (austenitic, ferritic and duplex), produced by cold-forming, considering a range of length from short to long columns. In the parametric study, the pin-ended boundary conditions were adopted, making the effective buckling lengths (assuming full composite action of individual components) equal to the corresponding column lengths. As part of the parametric study, an additional FE study was conducted to investigate how the length of the end fastener group affects the strength of the built-up column in the intermediate and high slenderness domain. The obtained results are presented in Section 3.2.1.

3.1 Finite element modelling and validation

The FEM assumptions are described in this section. A 4-noded shell element S4R with hourglass control and reduced integration was employed to model the measured geometry of the individual components composing the built-up

specimens. A square mesh size of 4 mm was chosen to discretise the flat and corner parts of the modelled angle sections. Mesh refinement was done until acceptable convergence was reached. For each component, a mesh sensitivity study was performed with sizes 10 mm, 4 mm and 2 mm. A size of 4 mm was selected since it gave very similar results to those with 2 mm at much less computation costs. To account for the material nonlinearity, the measured stress–strain curves obtained through flat and corner tensile coupon tests (see Table 2) were used in the FE models. The corner material model was confined to the corner region as it was found that there are no significant strength increases beyond the curved portions in press-braked sections [31]. Poisson's ratio of 0.3 and Young's modulus value of 200 000 N/mm^2 were assumed. The nominal stress–strain curves were transformed into true stress–strain curves to be inputted in the ABAQUS plasticity model.

The surface-to-surface general contact interaction was selected to model the contact pairs between the abutting surfaces of the individual components. The property of the normal contact behaviour was defined as hard contact, whereas the tangential contact behaviour was modelled as penalty friction formulation, assuming a friction coefficient of 0.35 for all contact surfaces. The inclusion of surface-to-surface contacts requires iterations in each loading increment, which often increases the computational time and causes convergence issues. Thus, the geometrically and materially non-linear analysis with imperfections (GMNIA) was developed as quasi-static using the dynamic explicit solver and the variable non-uniform mass scaling technique was used to shorten the computational time. Mass scaling with a time increment of $5x10^{-6}$s was used in the analyses. A smooth loading amplitude is automatically created when using the explicit dynamic process in Abaqus to avoid large inertial forces in the quasi-static analysis. In this process, applying the load in the "smoothest possible manner" requires that the acceleration changes only slightly from one step to the next. If the acceleration changes only slightly (is "smooth"), it follows that the displacement changes are also smooth.

The bolts were modelled as linear springs, using a mesh-independent connector element [32], [33], [34]. The bolt shear stiffness was defined as the slope of the linear portion of the load-displacement curve, beginning at 40% of the maximum load, see Fig. 2, to account for the shear slip between individual connected components [33]. The physical radius of the bolt was introduced by kinematically coupling all the nodes located on the physical radius with the end points of the connector.

For the validation step, the measured amplitudes and directions of the initial geometric imperfections were used. Geometric imperfections were considered by introducing the eigenmode shape obtained from linear bifurcation analysis (LBA) to the subsequent FE model where GMNIA was conducted. The eigenmode shape was scaled to achieve the maximum absolute value (amplitude). The measured overall geometric imperfections (from each tested group) were introduced in the corresponding models as linear combinations of wave sine functions which reflected the obtained LBA mode-shapes.

Replication of the boundary conditions of the built-up T-section specimens was implemented by coupling the nodes at the column ends to reference points, which were assigned displacement and rotation restraints as in the physical tests. Warping was also prevented at both ends. To simulate the supporting conditions of the built-up cruciform-section specimens, the end plates of the testing machine were modelled as 2D rigid bodies. Reference points were set at the centroid of the top and bottom rigid bodies. The only slave degree of freedom was translation along the column axial (longitudinal) direction at one end of the column. The surface-to-surface general contact was selected to model the interactions between the surfaces of the column end cross-sections and the end plates of the testing machine. Hard contact formulation for normal behaviour and penalty friction formulation for tangential behaviour (with a friction coefficient of 0.35) were used. To model the axial load applied, a longitudinal displacement was imposed at the end free to move longitudinally.

A summary of the comparisons between the FE model results and those obtained experimentally is presented in Fig. 16, Fig. 17, and Fig. 18. A reasonable agreement between the experimental and FE results was obtained in terms of ultimate buckling loads, overall curve shape, initial stiffness and deformation capacity. FTB and TB failure modes were successfully captured by the FEMs. The average numerical-to-experimental ultimate load is 1.01 with a coefficient of variation of 2.27 % (see Table 5).

Fig. 16d compares the distributions of the relative slip of the connected angle legs of the built-up T-section column ⊤ 80 × 4 – 1000 – 395 obtained in the experiment (measured by "shear slip" LVDTs in the EFG) and numerical modelling. For the FE model, the distribution of the relative shear slip was calculated as the difference of displacements between the contact surfaces of these individual components, by carefully selecting nodal displacements corresponding to the position of the LVDTs. The FE model indeed shows different longitudinal shear slip of the contact surfaces compared to the experiment. This could be due to the initial position of each individual component in relation to each other which introduces eccentricity. Differences in terms of shear slip, between the FE model and the experiment, are also due to the initial position of the bolt in the hole and the hand-tight conditions.

The comparisons demonstrate the ability of the developed FE models to predict the physical behaviour observed in the experiments and the suitability of their use in a subsequent parametric study.

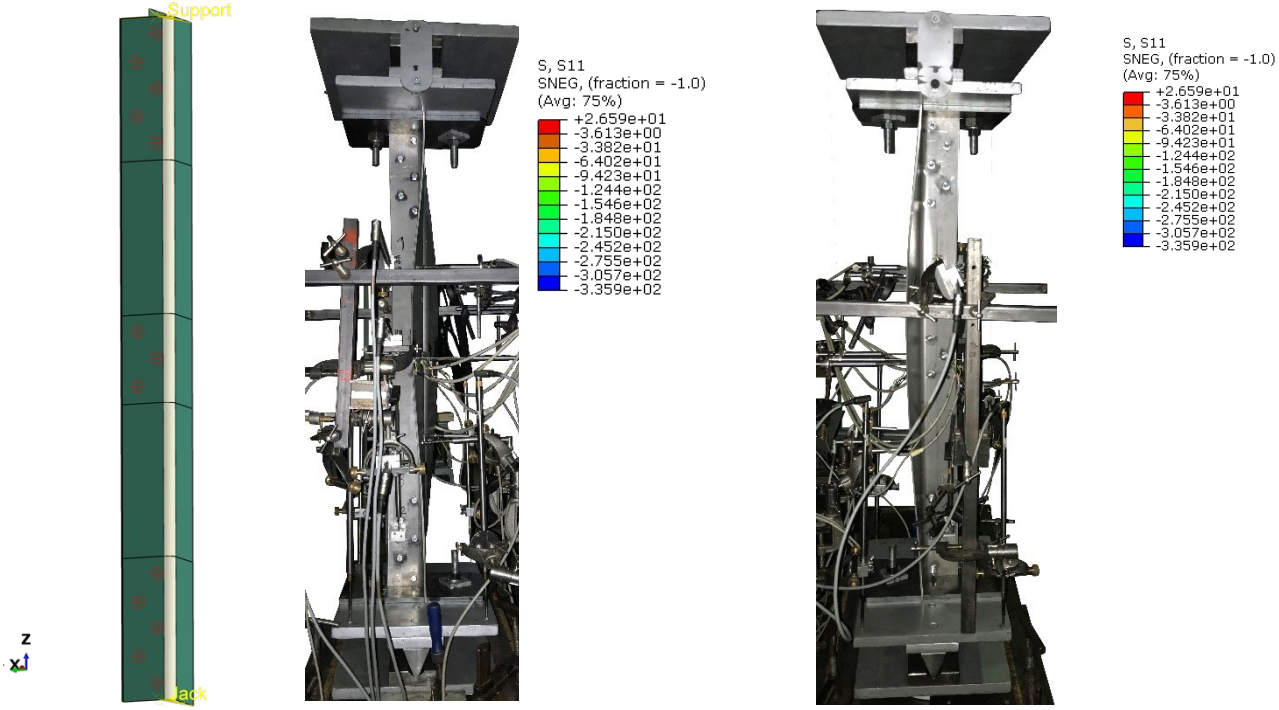

(*a*) FE built-up model (*b*) Buckling pattern – EXP versus FEM

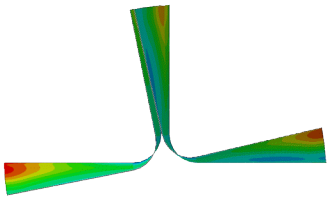

(*c*) deformed cross-section at peak load

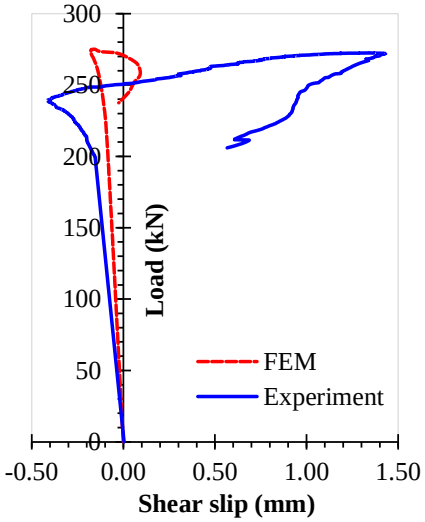

(*d*) Load versus shear slip curves

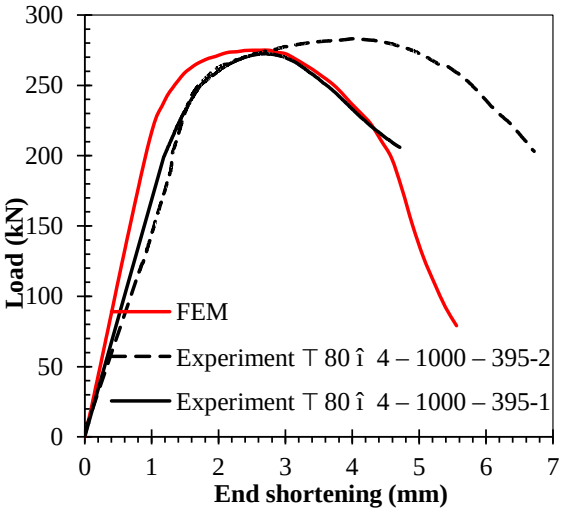

(*e*) Load versus end shortening curves

Fig. 16 Comparisons between FEM and experiment for built-up T-section column ⊤ 80 × 4 – 1000 – 395.

1

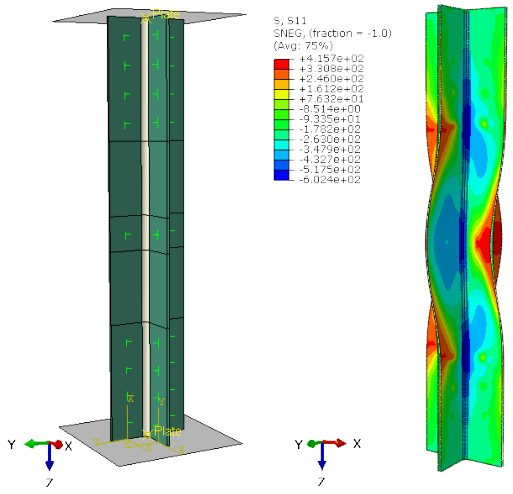

(*a*) FE built-up model (*b*) Buckling pattern

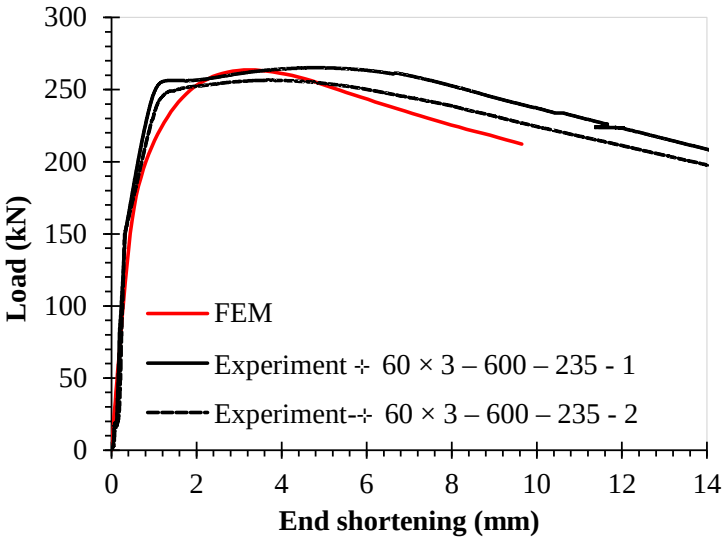

(*c*) Load versus end shortening curves

Fig. 17 Comparisons between FEM and experiment for built-up cruciform-section columns ÷ 60 × 3 – 600 – 235

2

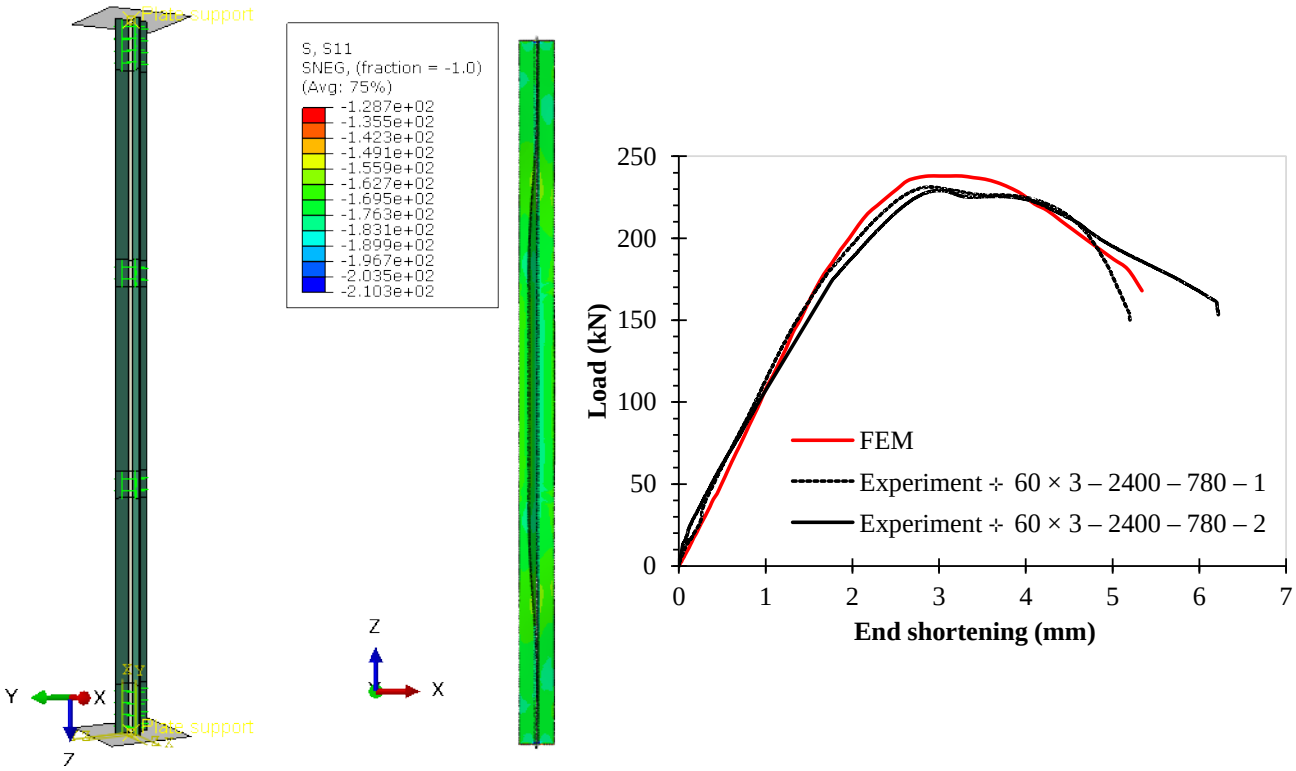

(*a*) FE built-up model (*b*) Buckling pattern (*c*) Load versus end shortening curves

Fig. 18 Comparisons between FEM and experiment for built-up cruciform-section columns ∔ 60 × 3 – 2400 – 780

Table 5 Comparison between the experimental failure loads and those obtained through FEMs.

Specimens	Governing failure mode	$P_{b,u,exp,mean}$ (kN)	$P_{b,u,FEM}$ (kN)	$P_{b,u,FEM}/P_{b,u,exp,mean}$
T 80 × 4 – 1000 – 395	FTB	277.8	275.0	0.990
∔ 60 × 3 – 600 – 235	TB	260.8	263.7	1.011
∔ 60 × 3 – 2400 – 780	TB	230.2	238.5	1.036
Mean				1.012
Coefficient of variation (%)				2.27

3.2 Parametric study

A parametric study was conducted using the validated FEM to obtain additional data related to the behaviours and ultimate buckling resistances of various CFSS built-up columns. Two built-up sections were considered in the study: T-section columns comprising two back-to-back equal-leg angles, and built-up cruciform-section columns comprising four star-oriented equal-leg angles, as it is shown in Fig. 19. Three different geometries of single equal-leg angle-section composing the built-up sections were considered: 60 × 4 mm, 80 × 4 mm, and 100 × 4 mm (constant values of the thickness t = 4 mm and internal radius r_i = 12 mm were adopted for all sections).

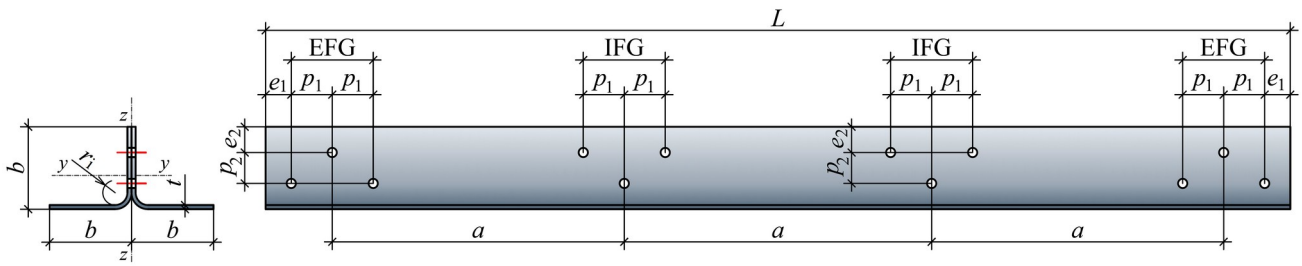

(*a*) Built-up T-section column comprising two back-to-back equal-leg angle components

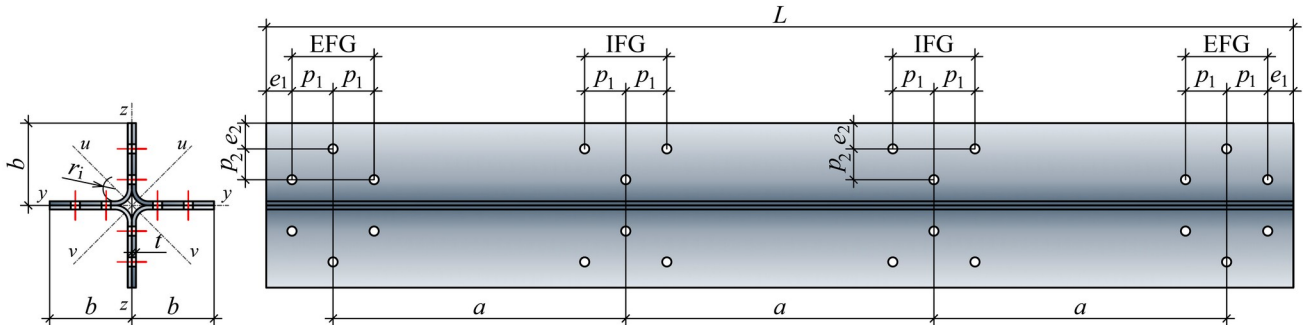

(*b*) Built-up cruciform-section column comprising four star-oriented equal-leg angle components

b − leg width of an individual angle section (*b* = 60 mm, *b* = 80 mm, *b* = 100 mm); *t* − wall thickness of an individual angle section (*t* = 4 mm); r_i − internal corner radius (r_i = 12 mm); *L* − built-up column length; *a* − centre-to-centre distance between two adjacent fasteners; *m* − the number of centre-to-centre distances between two adjacent fasteners; i_i − minimum radius of gyration of the cross-section of an individual angle; *i* − radius of gyration of the built-up section; e_1 − end distance; e_2 − edge distance; p_1 and p_2 − fastener spacings; EFG − end fastener group; EFG includes 2, 3, 4, 5, 6 or 7 fasteners in each connected leg; IFG − intermediate fastener group; IFG includes 2 or 3 fasteners in each connected leg.
For FE models ⊤60×4 and ÷60×4, e_1 = 25 mm, e_2 = 25 mm, and p_1 = 40 mm (bolt arrangement in one line).
For FE models ⊤80×4 and ÷80×4, e_1 = 25 mm, e_2 = 25 mm, p_1 = 40 mm, p_2 = 25 mm (staggered bolt arrangement).
For FE models ⊤100×4 and ÷100×4, e_1 = 25 mm, e_2 = 25 mm, p_1 = 40 mm, p_2 = 50 mm (staggered bolt arrangement).

Fig. 19 Nominal geometry and parameters designation for CFSS FE built-up columns in the parametric study (all dimensions in mm).

The individual angles are mutually connected by M8 bolts at the column ends and additionally at one third (or one half) of the column length — a staggered bolt arrangement was used for angles with leg widths of 80 mm and 100 mm, whereas one-line bolt arrangement was used for angle with leg width of 60 mm. The longitudinal bolt spacing was equal to 5 bolt diameters (p_1 = 5·8 mm = 40 mm) both for EFG and IFG, i.e., higher than 4 bolt diameters as prescribed in AISI-S100-16 Specification [18]. The number of IFGs along the length of the columns was 2 for most of the FE built-up columns, as it is a limitation prescribed in EN 1993-1-1 [14] (cases without IFG or with one IFG are explicitly listed in the footnotes of Table ii, Table iii and Table iv, at the end of this paper). The sensitivity study considers the influence of the number of fasteners in the end connections (2, 3, 5, 6, or 7 fasteners on each connected leg) and intermediate connections (2 and 3 fasteners on each connected leg) on the column ultimate buckling response. Based on the results obtained, the length of the end fastener group was adopted as 2*b* (2*b* is the maximum dimension of the built-up section) in the subsequent parametric study. A summary of the variation ranges for the key parameters is presented in Table i and Table ii for the duplex grade, and in Table iii and Table iv, for the austenitic and ferritic grades, respectively, at the end of this paper.

The influence of material nonlinearity on the column compressive strength was analysed for 3 primary stainless steel alloys, austenitic, ferritic, and duplex. Full stress-strain curves determined from flat and corner coupon tests were used for the austenitic and duplex alloys (see Table 2). The Ramberg-Osgood's model [26] was employed to simulate the material response for the ferritic alloy [35] whereas Rossi's predictive model [31] was used to account for the strain-hardening effects in the corner regions caused by press-braking.

Initial geometric imperfections, considered in the FE study, include bi-planar out-of-straightness, twist imperfection and out-of-flatness of angle legs. Considering that the local- and torsional-buckling modes of equal-leg angle sections feature similar deformed shapes, a single initial twist imperfection was considered herein to trigger both modes: a sinusoidal half wave mode shape over the column length, reflecting twist eigenmode shape, with an amplitude of $\tan^{-1}(L/1000b)$ at the column mid-height [36]. The amplitude of a thousandth of the column height was adopted about both principal axes for the initial out-of-straightness. Superposition of the initial geometric imperfections was introduced in each FE model; depending

on the column slenderness, one of the imperfections was used as the leading and the other was reduced by a factor equal to 0.7 as per [37], [38].

The general labelling convention of test specimens was also used to refer to each FE model.

3.2.1 Effect of fastener group lengths on buckling responses

The FE sensitivity study, covering the intermediate and high slenderness domain of CFSS T- and cruciform-section built-up columns was performed to investigate the influence of fastener group lengths (the number of fasteners in the connection) on the column ultimate responses. The dimensions of the considered single angle-sections, which form the built-up columns, are 80 × 4 mm and 100 × 4 mm. The FE sensitivity study was performed only for the duplex grade. The ultimate capacities $P_{b,u,FEM}$ and failure modes obtained in this study are summarised in Table i.

It can be seen from Table i that the failure modes and ultimate buckling strengths of T- and cruciform-section columns with EFG length equal to 2*b* or 1.5 times 2*b* (the last is according to AISI-S100-16 [18]) are almost the same, in the intermediate and high slenderness domain (in both cases the longitudinal spacing between bolts is equal to 5 bolt diameters). Besides, a change in intermediate fastener group length (from 0.2 times 2*b* to 0.5 times 2*b*) does not affect the ultimate response of these columns. Compared to the rule in AISI-S100-16 [18], this finding can be attributed to the higher shear stiffness of bolted connections compared with connections with screws.

A drop of ultimate buckling load was noticed only in cruciform-section built-up columns of intermediate length with EFG length equal to 0.2 times 2*b* or 0.4 times 2*b*. However, this is noticeable only for cruciform columns with wider legs featuring dominantly torsional deformations (the angle section is 100 × 4 mm), for which the ultimate buckling loads are lower by up to 19% compared with columns with EFG length equal to 2*b*. The explanation for these behavioural differences cannot be entirely based on the number of fasteners used in the EFGs to connect the individual components (which are most effective in the case of a built-up column that buckles in a flexural mode). Indeed, because wider cross-section walls are more prone to instability than shorter ones, the impact of local instability on the ultimate buckling behaviours of these columns cannot be neglected. Each leg of a cruciform-section behaves like a plate with one longitudinal edge supported and the other one free. The boundary conditions (associated with rotational restraints) along the longitudinal edge strongly depend on the slenderness (hence flexibility) of the other 3 legs. The boundary conditions influence the distributions and intensity of the compressive stresses, but also the amount of shear deformations caused by bending of the individual legs in the critical cross-section. In general, under pure axial compression, the restrained outstand section part is subjected to transverse bending and buckles in several half-waves (local mode). On the contrary, in the absence of restraint, the "pinned" outstanding section part does not transversally bend and buckles in a single half-wave (torsional mode), regardless of its slenderness. This means that the shear stiffness of the connections along the column lengths (also along the leg widths) is crucial in maintaining the integrity of the built-up column undergoing twisting (avoiding separation of the individual components and their independent behaviours). This observation is particularly related to the fasteners placed where the torsional deformations attain their maximum (typically near the mid-height of the column).

In addition, it is worth noting that the structural behaviour of axially compressed stainless steel columns in the low and intermediate slenderness domain is also influenced by material nonlinearity (the gradual yielding between the “proportionality” stress and yield strength leads to softening of the material, thus causing a potential drop of ultimate buckling resistance).

In view of what was previously mentioned, it was found that the influence of the amount of fastener in the end fastener groups on the buckling behaviour is less pronounced for built-up T-section with intermediate length: in comparison with columns with EFG length equal to 2*b*, the ultimate buckling loads are lower by up to 6%. This can be attributed to the fact that their structural response is simultaneously affected by dominant major-axis flexural-torsional behaviour (the major-axis lies in the connection plane of individual components) and the less dominant minor-axis flexural behaviour (out of the connection plane) that can beneficially affect the overall column deformations and reduce shear forces in the connections.

3.2.2 Failure behaviour and ultimate buckling loads as results of the parametric study

The ultimate buckling loads $P_{u,FEM}$ and failure modes of FE CFSS built-up columns considered in this parametric study are presented for duplex, austenitic and ferritic grades in Tables ii, iii and iv respectively. As shown in the Tables, the parametric study was conducted on built-up columns with various lengths and bolt group spacings. The EFG length of each column was adopted as the maximum dimension of the built-up section, with the longitudinal spacing between bolts equal to 5 bolt diameters. The failure buckling mode of each column was thoroughly analysed and established based on the stress and displacement distributions. Ultimate buckling patterns for 3 selected FE columns are shown in Fig. 20. The distribution of the longitudinal shear slip between the connected surfaces at the EFG position, for a selection of built-up T- and cruciform-sections columns, are shown in Fig. 21.

The observation of the buckling results leads to the following comments:

(i) The adopted fastener arrangement between the component equal-leg angle built-up T- and cruciform-sections enables a sufficient level of composite action; the separation of individual components, distortions and local deformations of the built-up cross-section was not found in the pre-peak elastic regime and ultimate load regime.

(ii) The ultimate buckling responses of built-up singly-symmetric T-section columns depend on their global slenderness and on the cross-section leg slenderness (leg width): for low and intermediate global slenderness, columns buckle in major-axis flexural-torsional buckling mode (involving flexure about the symmetry axis which is the major cross-sectional principal axis); for the high slenderness domain, buckling occurs in interactive major-axis flexural–torsional and minor-axis flexural modes.

(iii) The ultimate buckling responses of built-up cruciform-section columns depend on their global slenderness, and on the cross-section leg slenderness (leg width): for low and intermediate global slenderness, columns buckle in a purely torsional mode, whereas for very long columns buckling takes place in a pure flexural mode about the principal *v*-*v* axis.

(iv) All columns display similar buckling behavioural features: the ultimate buckling load decreases monotonically with the column length; the torsional mode almost always plays a key role: it participates in the critical buckling modes of all but the very long columns.

(v) When compared to the singly-symmetric built-up T-section column, the built-up cruciform-section column, with the same individual equal-leg angle component and length, exhibits higher ultimate buckling load: the ultimate buckling load ratios range from 1.86 to 3.64, 1.86 to 2.78, and 1.80 to 2.97 for the duplex, ferritic, and austenitic grades, respectively (the cross-sectional area of the cruciform-section is 2.0 times that of the T-section).

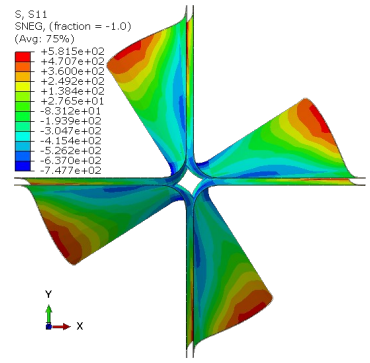

(*a*) TB failure mode of duplex CFSS built-up column ÷100×4×1500-625-2

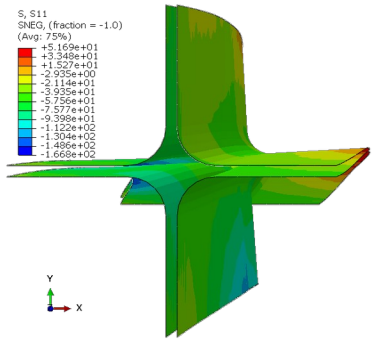

(*b*) FB about *u*-*u* / *v*-*v* axis failure mode of ferritic CFSS built-up column ÷60×4×4400−1425−3

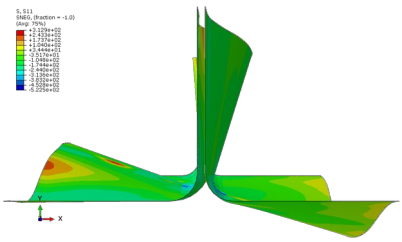

(*c*) FTB failure mode of ferritic CFSS built-up column ⊤100×4×2500−770−3

Fig. 20 Failure modes of selected FE CFSS built-up columns.

1

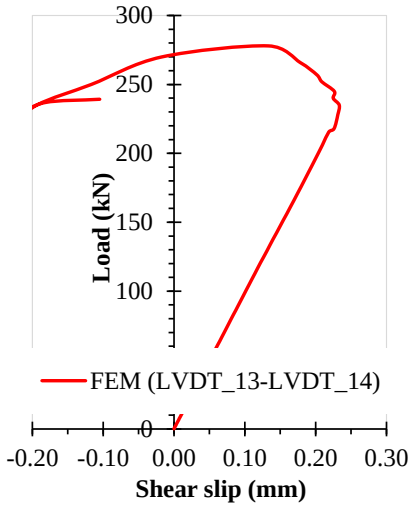

(*a*) ⊤80×4×1000−395−2

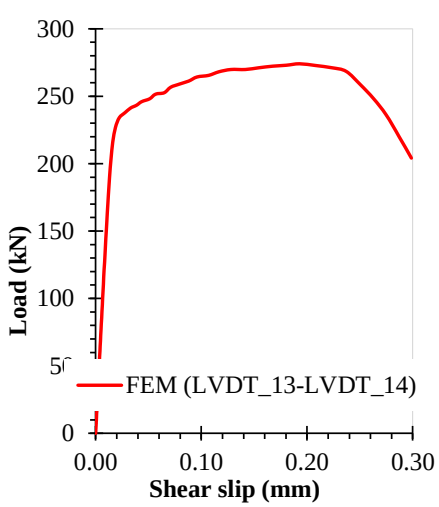

(*b*) ⊤80×4×1000−435−2

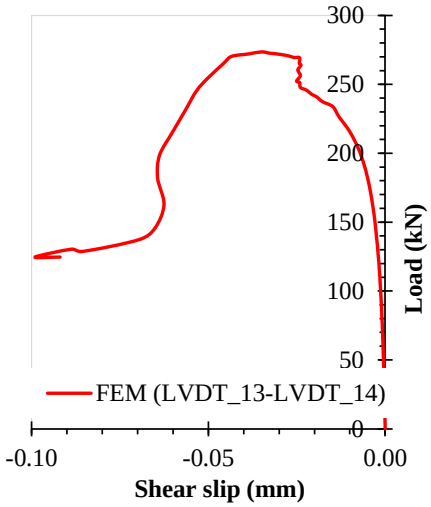

(*c*) 80×4×1000−455−2

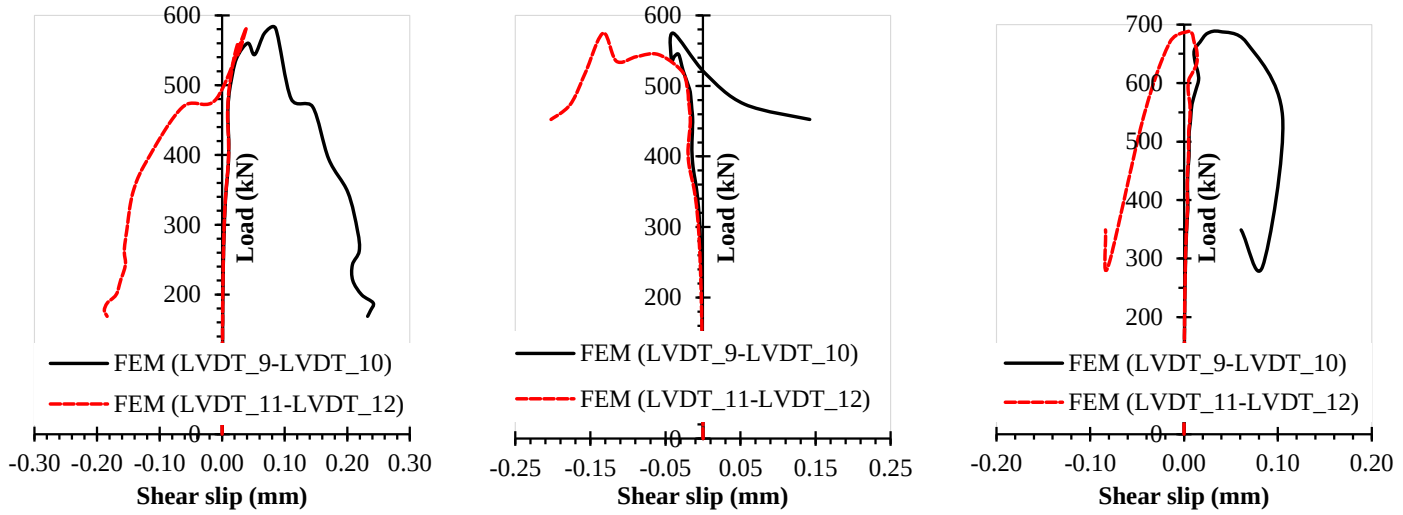

(*d*) ÷100×4×2000−955−2 (*e*) ÷100×4×2000−935−2 (IFG 1×40=40) (*f*) ÷100×4×2000−835−2 (IFG 1×40=40)

*Designations of FE models are as in Table i

Fig. 21 Load versus shear slip curves in FEM

4 Accuracy assessment of design recommendations for built-up section columns

This chapter includes the accuracy assessment of the current Direct Strength Method (DSM) stated in AISI-S100-16 [18] for the CFSS built-up T- and cruciform-section columns, numerically analysed in Section 3, including the effective rigidities (EI_{eff}, $EI_{w,eff}$, GJ_{eff}) recently proposed for built-up columns comprising three or more component sections and failing in flexural or flexural-torsional global modes [4], [5].

Comparisons of the FE results are also made against the design provisions based on the modified slenderness approach stated in Section 5.4.2 EN 1993-1-4 [13], and in Section E.6, ANSI/AISC 370-21 [15]. Note that the existing code EN 1993-1-4 [13] does not explicitly state the values of the imperfection factor α nor the limiting slenderness $\overline{\lambda}_0$ for CFSS angle-section. Thus, according to the Design Manual for Structural Stainless Steel [39], the conservative buckling curve *d* with the imperfection factor α = 0.76 and a non-dimensional limiting slenderness $\overline{\lambda}_0$ = 0.2 was employed herein for CFSS built-up members.

The FE results were carefully considered to clearly identify the failure modes; the failure mode governed by dominant TB, FTB or FB was selected to evaluate the corresponding design failure load. For cases in which TB and FTB were the critical mode, the accuracy assessment included the use of the gross cross-sectional areas for all column capacity calculations to avoid double-accounting of local/torsional buckling [36], [40]. The safety factors were taken equal to 1.0 in the predictions of the ultimate column resistances for each design method.

A comparison of the generated FE data with the design data is presented in Fig. 22 and Fig. 23 for CFSS built-up T- and cruciform-section columns, respectively, using different colour coding for each design procedure. In the figures, a distinction is made between the austenitic, ferritic, and duplex stainless steel grades. The statistical indicators, average values, Coefficient of Variations (CoVs) and maximum / minimum values, concerning the failure loads, are also provided for each design procedure.

4.1 Design procedure based on DSM and effective rigidities

As mentioned above, Phan et al. [4], [5] have recently developed, validated and proposed a novel DSM-based procedure for the design of CFS fixed-ended and pin-ended built-up columns exhibiting FB or FTB mode. The design procedure recommends the use of the current Direct Strength Method and effective flexural, torsional and warping rigidities for the design of columns susceptible to flexural or flexural-torsional buckling modes. The fastener spacing limit $\left(a/i_{\mathrm{i}}\right)/\left(kL/i\right)\le 0.5$ (where *k* is the buckling length factor) is utilised.

According to the DSM specified in E3.2, AISI-S100-16 [18], the nominal axial strength P_{n} of a compression member should be determined as the minimum of the nominal column strengths for global (flexural, torsional or flexural-torsional) buckling P_{ne}, local buckling P_{nl} and distortional buckling P_{nd}. The nominal column strength for global buckling is determined as follows:

$$P_{\mathrm{ne}}=A_{\mathrm{g}}f_{\mathrm{n}} \tag{1}$$

where A_{g} is the gross area, and f_{n} is the global column stress:

$$f_{\mathrm{n}}=\begin{cases}\left(0.658^{\lambda_{\mathrm{c}}^{2}}\right)f_{\mathrm{y}} & \text{for } \lambda_{\mathrm{c}}\le 1.5\\ \left(\dfrac{0.877}{\lambda_{\mathrm{c}}^{2}}\right)f_{\mathrm{y}} & \text{for } \lambda_{\mathrm{c}}>1.5\end{cases} \tag{2}$$

where $\lambda_{\mathrm{c}}=\sqrt{f_{\mathrm{y}}/f_{\mathrm{cre}}}$ and f_{cre} is the minimum of the elastic critical FB, TB and FTB stresses, determined using formulae defined in Sections E2.1 and E2.2, AISI-S100-16 [18].

The nominal column strength for local buckling P_{nl} is determined as follows:

$$P_{\mathrm{nl}}=\begin{cases}P_{\mathrm{ne}} \text{ for } \lambda_{\mathrm{l}}\le 0.776\\ \left[1-0.15\left(\dfrac{P_{\mathrm{crl}}}{P_{\mathrm{ne}}}\right)^{0.4}\right]\left(\dfrac{P_{\mathrm{crl}}}{P_{\mathrm{ne}}}\right)^{0.4}P_{\mathrm{ne}} \text{ for } \lambda_{\mathrm{l}}>0.776\end{cases} \tag{3}$$

where $\lambda_{\mathrm{l}}=\sqrt{P_{\mathrm{ne}}/P_{\mathrm{crl}}}$, $P_{\mathrm{crl}}=A_{\mathrm{g}}f_{\mathrm{ol}}$, f_{ol} is the elastic local buckling stress.

The nominal column strength for local distortional P_{nd} is determined as follows:

$$P_{\mathrm{nd}}=\begin{cases}P_{\mathrm{y}} \text{ for } \lambda_{\mathrm{d}}\le 0.561\\ \left[1-0.25\left(\dfrac{P_{\mathrm{crd}}}{P_{\mathrm{y}}}\right)^{0.6}\right]\left(\dfrac{P_{\mathrm{crd}}}{P_{\mathrm{y}}}\right)^{0.6}P_{y} \text{ for } \lambda_{d}>0.561\end{cases} \tag{4}$$

where $\lambda_{\mathrm{d}}=\sqrt{P_{\mathrm{y}}/P_{\mathrm{crd}}}$, $P_{\mathrm{y}}=A_{\mathrm{g}}f_{\mathrm{y}}$ and $P_{\mathrm{crd}}=A_{\mathrm{g}}f_{\mathrm{od}}$, f_{od} is the elastic distortional buckling stress.

The elastic local and distortional buckling stresses were determined numerically using the computer program CUFSM [23].

When determining the nominal axial strength P_{n}, the effective second moments of area $I_{\mathrm{y,eff}}\left(I_{\mathrm{u,eff}}\right)$ and $I_{\mathrm{z,eff}}$ $\left(I_{¿¿\ \mathrm{v,eff}}\right)¿$ for the major and minor principal axes should be obtained as follows:

$$I_{\text{eff}} = \alpha I_{\text{full}} \tag{5}$$

The effective warping constant $I_{\text{w,eff}}$ should be obtained as follows:

$$I_{\text{w, eff}} = \alpha I_{\text{w,full}} \tag{6}$$

while the parameter α in Eqs. (5) and (6) should be determined as follows:

$$\alpha = \frac{\left(\frac{kL}{i}\right)_0^2}{\left(\frac{kL}{i}\right)_0^2 + \left(\frac{a}{i_{\text{i}}}\right)^2} \tag{7}$$

where ¿ is the global slenderness ratio of the entire section about the built-up member axis, and a/i_{i} is the individual component slenderness ratio.

The effective torsion constant J_{eff} and the effective local $f_{\text{ol, eff}}$ and distortional $f_{\text{od, eff}}$ buckling stresses should be obtained as follows:

$$J_{\text{eff}} = n J_{\text{ind}} \tag{8}$$

$$f_{\text{ol, eff}} = f_{\text{ol,ind}} \tag{9}$$

$$f_{\text{od, eff}} = f_{\text{od,ind}} \tag{10}$$

Subscripts "*ind*" and "*full*" indicate the values for a single independent section and the built-up section assuming full composite action, respectively; n is the number of single sections composing the built-up section [4], [5].

4.2 Comparisons

Comparisons of the FE ultimate capacities $P_{\text{u,FEM}}$ with the predicted design resistances $P_{\text{u,pred}}$ according to DSM-based design approach [4], [5], EN 1993-1-4 [13] and ANSI/AISC 370-21 [15] codified procedures, together with the statistical indicators on the failure loads, are graphically shown in Fig. 22 and Fig. 23 for CFSS built-up T-section columns and CFSS built-up cruciform-section columns, respectively. In the graphs, $\overline{\lambda}$ is the non-dimensional relative slenderness about *y-y* axis.

In general, the trend lines shown in the graphs achieve their minima in the transition range between the TB or FTB and FB modes. The FE failure loads are generally underestimated by both EN 1993-1-4 [13] and ANSI/AISC 370-21 [15] design procedures, with a large margin and scatter in the data, especially for CFSS built-up cruciform-section columns. Compared to these design procedures, the proposed DSM-based design approach [4], [5] yields more accurate predictions of the ultimate column strengths, especially in the case of CFSS built-up T-section columns that failed dominantly by FTB. The assessment of the design methods also shows that the highest data scatter was found for duplex stainless steel.

5 Conclusions

This paper first presents a series of tests used to validate a FE model. The repeated compression tests were conducted on short (1000 mm) pin-ended built-up T-section specimens made of lean-duplex stainless steel grade EN 1.4162, and short (600 mm) and long (2400 mm) built-up cruciform-section specimens made of austenitic stainless steel grade EN 1.4301.

The individual cold-formed angle components were connected using M8 bolts, class 8.8 with a 1 mm bolt-to-hole clearance. Then a parametric study on CFSS built-up T- and cruciform-sections formed with two or four equal-leg angle sections failing by FTB, TB and FB, or their interactions, follows. The FE parametric study comprised 147 built-up T- and 161 built-up cruciform-section columns with pin-ended boundary conditions, covering a slenderness range (about the minor-principal axis of the built-up section assuming full composite action) from 0.3 to 3.5. Austenitic, ferritic, and duplex stainless steel grades were included in the parametric study.

The following main conclusions could be drawn from the study:

1. Major-axis FTB was the primary limit state for the built-up T-section specimens, whereas the built-up cruciform-section specimens failed due to TB. However, for longer built-up cruciform-section specimens, FB and LB were also captured, which illustrated the nature of coupled instability. For all specimens, the number of fasteners along the specimen length ensured that the individual components maintained unified structural integrity throughout testing; avoiding premature buckling failure of individual components. The critical cross-sections (at mid-length), experienced “rigid-body” like rotation accompanied by transverse bending of the individual angle legs. Bending deformations of slender outstand legs are pronounced in the portion between two adjacent fastener rows indicating local buckling — this is due to smaller rotational restraint stemming from the absence of fasteners.

2. As derived from the parametric study on pin-ended built-up T- and cruciform-section columns, an increase in the number of fasteners in the end fastener groups provides the largest strength improvements for the intermediate length built-up cruciform-section columns with wide legs, exhibiting TB failure mode. The strength improvements strongly depend on the level of rotational restraints of each cross-section leg associated with their slenderness, and consequently on the amount of the shear deformations caused by bending of the individual legs in the critical cross-section. This means that the shear stiffness of the connections along the column lengths (and along the leg widths) is crucial in maintaining the integrity of the built-up column undergoing twisting; this observation is particularly related to fasteners placed where the torsional deformations attain their maximum. The influence of the amount of fastener in the end fastener groups is less pronounced on the buckling behaviour of built-up T-section with intermediate length. This can be attributed to the fact that the structural response of these columns is simultaneously affected by the dominant major-axis flexural-torsional behaviour and the less dominant minor-axis flexural behaviour that may beneficially affect the overall column deformations and reduce shear forces in the connections. The influence of the rotational restraint of wide outstanding parts of built-up columns (also related to fastener positions along the column length) failing in the TB or FTB modes raises interesting issues and requires further studies.

3. The paper continues with an assessment of the accuracy of the DSM-based design method [4], [5], recently developed for the design of CFS fixed-ended and pin-ended built-up columns exhibiting FB or FTB modes, expressed in terms of the effective cross-section rigidities. It was shown that the FE failure loads obtained in this study are safely and reasonably accurately predicted by this approach, thus providing further evidence of its merits for nonlinear stress-strain materials as well. However, the prediction accuracy is lower in the case of CFSS built-up cruciform-section columns exhibiting dominant torsional failure deformations. TB interacting combined with LB appears for slender cruciform-section columns with two IFGs (e.g., ÷100×4×6100−1970−3). However, for these FE columns (for all three grades), the DSM-based design method also appears to provide an acceptable degree of accuracy in predicting their carrying capacity. In addition, the column failure loads were also used to assess the performance of the design procedures prescribed in EN 1993-1-4 [13]

(where an imperfection factor α = 0.76 in conjunction with a non-dimensional limiting slenderness $\overline{\lambda}_0$ = 0.2 were used), and ANSI/AISC 370-21 [15]. Both European and North American Specifications were shown to be conservative with higher scatter, thereby demonstrating a need for improvement.

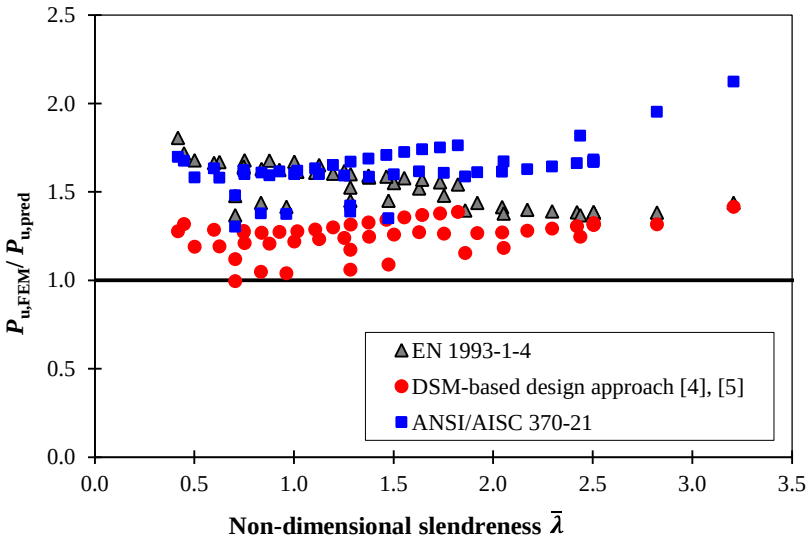

DSM-based design approach [4], [5]
Average 1.254
CoV 7.37%
Max 1.42
Min 1.00

EN 1993-1-4 [13]
Average 1.531
CoV 7.71%
Max 1.81
Min 1.37

ANSI/AISC 370-21 [15]
Average 1.606
CoV 6.58%
Max 1.80
Min 1.30

(*a*) Austenitic grade

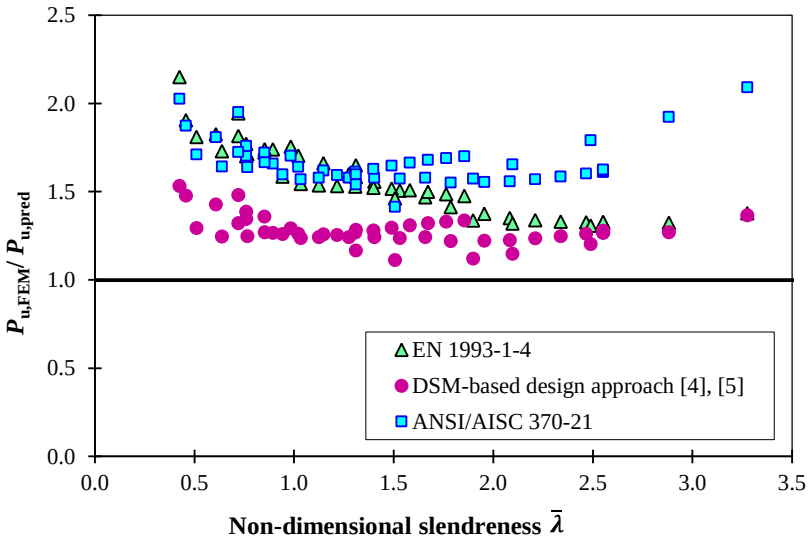

DSM-based design approach [4], [5]
Average 1.281
CoV 6.38%
Max 1.53
Min 1.11

EN 1993-1-4 [13]
Average 1.559
CoV 12.70%
Max 2.15
Min 1.31

ANSI/AISC 370-21 [15]
Average 1.641
CoV 6.84%
Max 2.03
Min 1.41

(*b*) Ferritic grade

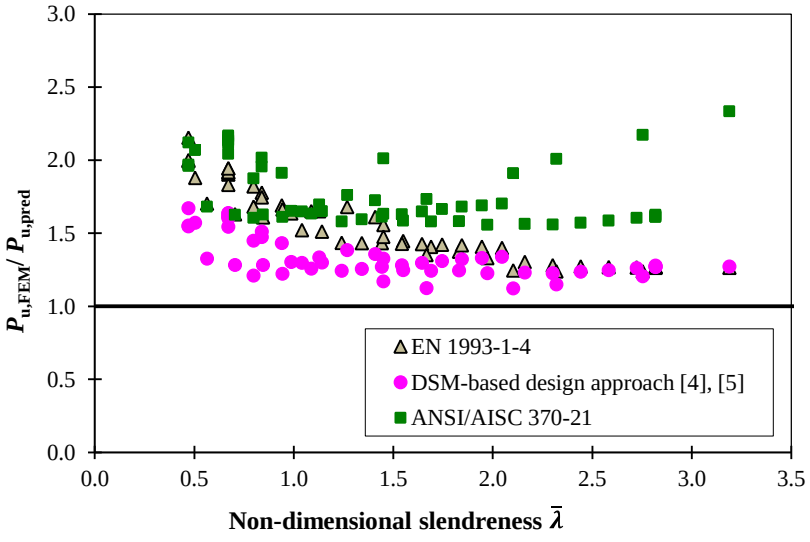

DSM-based design approach [4], [5]
Average 1.340
CoV 10.67%
Max 1.67
Min 1.12

EN 1993-1-4 [13]
Average 1.546
CoV 15.99%
Max 2.15
Min 1.24

ANSI/AISC 370-21 [15]
Average 1.792
CoV 13.33%
Max 2.54
Min 1.56

(*c*) Duplex grade

Fig. 22 Comparisons between FE and design capacities for CFSS built-up T-section columns.

1

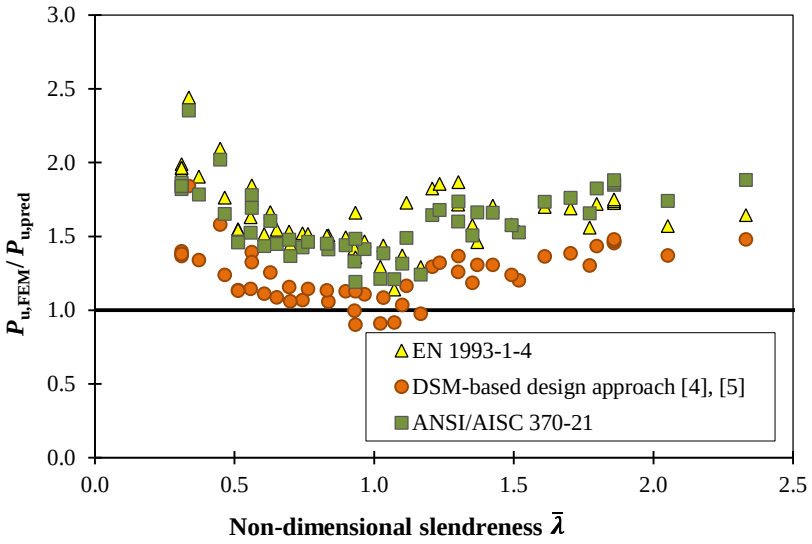

DSM-based design approach [4], [5]
Average 1.246
CoV 14.92%
Max 1.84
Min 0.90

EN 1993-1-4 [13]
Average 1.650
CoV 13.73%
Max 2.44
Min 1.14

ANSI/AISC 370-21 [15]
Average 1.607
CoV 14.41%
Max 2.36
Min 1.19

(*a*) Austenitic grade

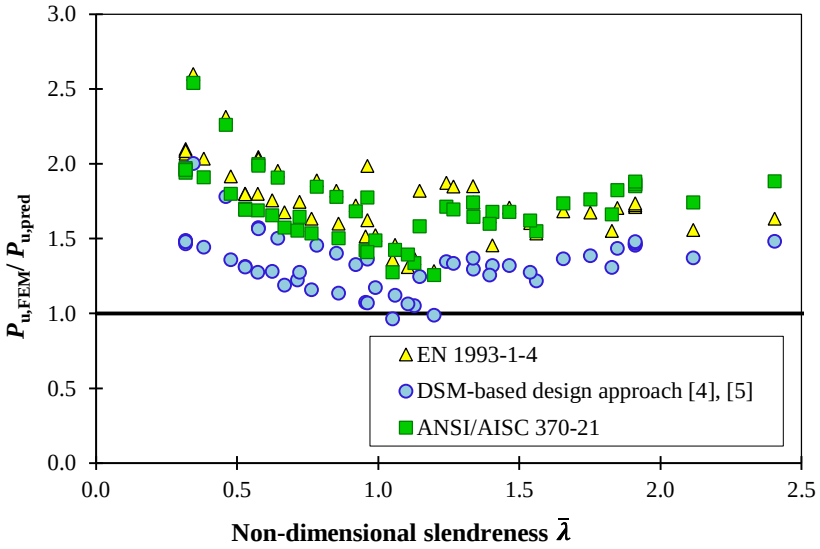

DSM-based design approach [4], [5]
Average 1.338
CoV 13.95%
Max 2.0
Min 0.97

EN 1993-1-4 [13]
Average 1.756
CoV 14.25%
Max 2.6
Min 1.29

ANSI/AISC 370-21 [15]
Average 1.721
CoV 13.59%
Max 2.54
Min 1.26

(*b*) Ferritic grade

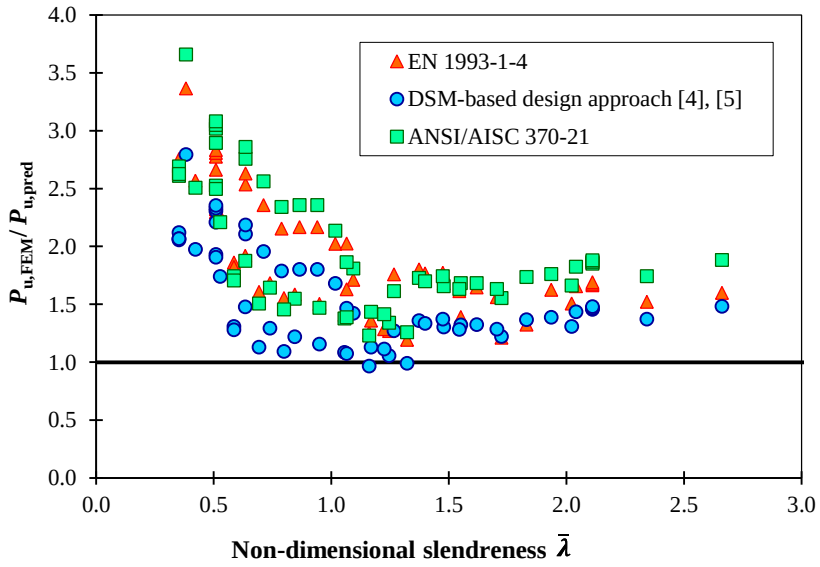

DSM-based design approach [4], [5]
Average 1.557
CoV 26.98%
Max 2.79
Min 0.97

EN 1993-1-4 [13]
Average 1.92
CoV 26.95%
Max 3.36
Min 1.19

ANSI/AISC 370-21 [15]
Average 2.002
CoV 27.75%
Max 3.66
Min 1.23

(*c*) Duplex grade

Fig. 23 Comparisons between FE and design capacities for CFSS built-up cruciform-section columns.

Acknowledgements

This investigation is supported by the Serbian Ministry of Education, Science and Technological Development through the 200092 project.

The authors are grateful to company AluBuild Engineering doo Belgrade and Institute for Testing of Materials Belgrade for their support.

References

[1] B. Rossi, Discussion on the use of stainless steel in constructions in view of sustainability, Thin-Walled Struct. 83 (2014) 182-189.

[2] F. Bleich, Buckling Strength of Metal Structures, McGraw-Hill Book Company, 1952.

[3] K.J.R. Rasmussen, M. Khezri, B.W. Schafer, H. Zhang, The mechanics of built-up cold-formed steel members, Thin-Walled Structures. 154 (2020) 106756.

[4] D.K. Phan, K.J.R. Rasmussen, B.W. Schafer, Tests and design of built-up section columns, J. Construct. Steel Res. 181 (2021) 106619.

[5] D.K. Phan, K.J.R. Rasmussen, B.W. Schafer, Numerical investigation of the strength and design of cold-formed steel built-up columns, J. Construct. Steel Res. 193 (2022) 107276.

[6] J. Becque, K.J.R. Rasmussen, Experimental investigation of the interaction of local and overall buckling of stainless steel I-columns, J. Struct. Eng. 135 (11) (2009) 1340–1348.

[7] F.J. Meza, J. Becque , I. Hajirasouliha, Experimental study of the cross-sectional capacity of cold-formed steel built-up columns, Thin–Walled Structures 155 (2020) 106958.

[8] F.J. Meza, J. Becque, I. Hajirasouliha, Experimental study of cold-formed steel built-up columns, Thin-Walled Structures. 149 (2020), 106291.

[9] D.C. Fratamico, S. Torabian, K.J.R. Rasmussen, B.W. Schafer, Buckling and collapse behavior of screw-fastened, built-up cold-formed steel columns of varying cross-section size: experimental investigation, Proceedings of the Annual Stability Conference, Structural Stability Research Council, San Antonio, Texas, March 21-24, 2017.

[10] D.C. Fratamico, S. Torabian, X. Zhao, K.J.R. Rasmussen, B.W. Schafer, Experimental study on the composite action in sheathed and bare built-up cold-formed steel columns, Thin-Walled Structures. 127 (2018) 290-305.

[11] Q. Li, B. Young, Experimental and numerical investigation on cold-formed steel built-up section pin-ended columns, Thin-Walled Structures. 170 (2022) 108444.

[12] S. Selvaraj, M. Madhavan, Experimental investigation and design considerations on cold-formed steel built-up I-section columns subjected to interactive buckling modes, Thin-Walled Structures. 175 (2022) 109262.

[13] Eurocode 3: Design of steel structures – part 1-4: General rules – supplementary rules for stainless steels, including amendment A1 (2015), EN 1993-1-4:2006+A1:2015, Brussels, Belgium, CEN 2015.

[14] Eurocode 3: Design of steel structures – Part 1-1: General rules and rules for buildings EN 1993-1-1, Brussels, Belgium, CEN 2005.

[15] Specification for Structural Steel Buildings. An American National Standard ANSI/AISC 370-21, American Institute of Steel Construction (AISC), Chicago, IL., June 11, 2021.

[16] Specification for Structural Steel Buildings. An American National Standard ANSI/AISC 360-16, American Institute of Steel Construction (AISC), Chicago, IL., July 7, 2016.

[17] Specification for the Design of Cold-Formed Stainless Steel Structural Members. ASCE Standard SEI/ASCE 8-02, American Society of Civil Engineers, Reston, VA, 2002.

[18] AISI-S100-16 (2016), North American Specification for the Design of Cold-Formed Steel Structural Members, AISI Standard, American iron and Steel Institute.

[19] J. Dobrić, A. Filipović, Z. Marković, N. Baddoo, Structural response to experimental axial testing of cold-formed stainless steel equal angle columns, Thin-Walled Struct., 156 (2020) 1-16.

[20] A. Filipović, J. Dobrić, N. Baddoo, P. Može, Experimental response of hot-rolled stainless steel angle columns, Thin-Walled Structures, 163 (2021) 107659.

[21] A. Filipović, J. Dobrić, D. Buđevac, N. Fric, N. Baddoo, Experimental study of laser-welded stainless steel angle columns, Thin-Walled Structures, 164 (2021) 107777.

[22] EN 10088-4: Stainless steels - Part 4: Technical delivery conditions for sheet/plate and strip of corrosion resisting steels for construction purposes. Brussels, Belgium, CEN 2009.

[23] Schafer BW, Ádány S. Buckling analysis of cold-formed steel members using CUFSM: conventional and constrained finite strip methods. In: Proceedings of the eighteenth international speciality conference on cold-formed steel structures. Orlando (USA); 2006.

[24] Eurocode 3, Design of Steel Structures – Part 1-8: Design of joints EN 1993-1-8, CEN, Brussels, Belgium, 2005.

[25] EN ISO 6892-1. Metallic materials – Tensile testing. Part 1: Method of test at room temperature. Brussels, Belgium, CEN 2009.

[26] I. Arrayago, E. Real, L. Gardner, Description of stress-strain curves for stainless steel alloys, Materials and Design. 87 (2015) 540-552.

[27] ECCS TC7, The Testing of Connections with Mechanical Fasteners in Steel Sheeting and Sections, (2009).

[28] D.C. Fratamico, S. orabian, X. Zhao, K.J.R. Rasmussen, B.W. Schafer, Experimental study on the composite action in sheathed and bare built-up cold-formed steel columns, Thin-Walled Structures. 127 (2018) 290–305.

[29] A. Landesmann, D. Camotim, P.B. Dinis, R. Cruz, Short-to-intermediate slender pin-ended cold-formed steel equal-leg angle columns: Experimental investigation, numerical simulations and DSM design, Engineering Structures 132 (2017) 471–493.

[30] ABAQUS User Manual, Version 6.12, Providence, RI, USA: DS SIMULIA Corp; 2012.

[31] B. Rossi, S. Afshan, L. Gardner, Strength enhancements in cold-formed structural sections – Part II: Predictive models, J. Constr. Steel Res., 83 (2013) 189–196.

[32] J. Dobrić, N. Gluhović, Z. Marković, D. Buđevac, Stability design criteria for closely spaced built-up stainless steel columns, Building Materials and Structures, vol. 64 (4) (2021) ISNN (online) 2335-0229, 235-250.

[33] D.K. Phan, K.J.R. Rasmussen, Flexural rigidity of cold-formed steel built-up members, Thin-Walled Struct. 140 (2019) 438–449.

[34] J.Ye, G.Quan, P. Kyvelou, L. Teh, L. Gardner, A practical numerical model for thin-walled steel connections and built-up members, Structures. 38 (2022) 753–764.

[35] B. Rossi, J.-P. Jaspart, K. J. Rasmussen, Combined distortional and overall flexural-torsional buckling of cold-formed stainless steel sections: Experimental investigations, Journal of Structural Engineering. 136 (4) (2010) 354–360.

[36] B. Behzadi-Sofiani, L. Gardner, M.A. Wadee, Stability and design of fixed-ended stainless steel equal-leg angle section compression members, Engineering Structures 249 (2021) 113281.

[37] Eurocode 3: Design of steel structures – Part 1-5: Plated structural elements EN 1993-1-5, Brussels, Belgium, CEN 2006.

[38] Execution of steel structures and aluminium structures – Part 2: Technical requirements for steel structures EN 1090-2, Brussels, Belgium, CEN 2008.

[39] Design Manual for Structural Stainless Steel First Edition, Fourth Edition, The Steel Construction Institute, 2017.

[40] J. Dobrić, A. Filipović, N. Baddoo, D. Buđevaca, B.Rossi, Design criteria for pin-ended hot-rolled and laser-welded stainless steel equal-leg angle columns, Thin-Walled Structures 167 (2021) 108175.

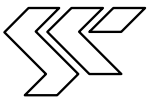

Annex

Table i Geometry and failure data of duplex CFSS FE built-up columns in the sensitivity study.

FE model	L (mm)	a (mm)	m	EFG (mm)	IFG (mm)	L/i	a/i_i	$\frac{a/i_i}{L/i}$	$P_{u,FEM}$ (kN)	Failure mode
T80×4×1000−395−2	1000	395	2	4×40=160	2×40=80	29.6	26.2	0.88	278.1	FTB
T80×4×1000−435−2	1000	435	2	2×40=80	2×40=80	29.6	28.8	0.97	268.7	FTB
T80×4×1000−435−2	1000	435	2	2×40=80	1×40=40	29.6	28.8	0.97	269.1	FTB
T80×4×1000−455−2	1000	455	2	1×40=40	1×40=40	29.6	30.2	1.02	268.1	FTB
T80×4×6000−1935−3	6000	1935	3	6×40=240	1×40=40	177.6	128.3	0.72	58.1	FTB + *y*−*y* axis FB
T80×4×6000−1930−3	6000	1930	3	6×40=240	2×40=80	177.6	128.0	0.72	58.8	FTB + *y*−*y* axis FB
T80×4×6000−1950−3	6000	1950	3	4×40=160	1×40=40	177.6	129.3	0.73	58.2	FTB + *y*−*y* axis FB
T80×4×6000−1970−3	6000	1970	3	4×40=160	2×40=80	177.6	130.6	0.74	58.4	FTB + *y*−*y* axis FB
T100×4×2000−955−2	2000	955	2	1×40=40	1×40=40	47.7	49.7	1.04	216.4	FTB
T100×4×2000−935−2	2000	935	2	2×40=80	1×40=40	47.7	48.7	1.02	226.6	FTB
T100×4×2000−935−2	2000	935	2	2×40=80	2×40=80	47.7	48.7	1.02	225.8	FTB
T100×4×2000−875−2	2000	875	2	5×40=200	2×40=80	47.7	45.6	0.95	229.4	FTB
T100×4×2000−835−2	2000	835	2	7×40=280	2×40=80	47.7	43.5	0.91	230.4	FTB
T100×4×2000−835−2	2000	835	2	7×40=280	1×40=40	47.7	43.5	0.91	228.3	FTB
÷80×4×1000−395−2	1000	395	2	4×40=160	2×40=80	29.6	26.2	0.88	754.4	TB
÷80×4×1000−435−2	1000	435	2	2×40=80	2×40=80	29.6	28.8	0.97	731.7	TB
÷80×4×1000−435−2	1000	435	2	2×40=80	1×40=40	29.6	28.8	0.97	735.7	TB
÷80×4×1000−455−2	1000	455	2	1×40=40	1×40=40	29.6	30.2	1.02	736.0	TB
÷80×4×6000−1935−3	6000	1935	3	6×40=240	1×40=40	177.6	128.3	0.72	124.2	*v*−*v* / *u*−*u* axis FB
÷80×4×6000−1930−3	6000	1930	3	6×40=240	2×40=80	177.6	128.0	0.72	123.7	*v*−*v* / *u*−*u* axis FB
÷80×4×6000−1950−3	6000	1950	3	4×40=160	1×40=40	177.6	129.3	0.73	123.8	*v*−*v* / *u*−*u* axis FB
÷80×4×6000−1970−3	6000	1970	3	4×40=160	2×40=80	177.6	130.6	0.74	123.9	*v*−*v* / *u*−*u* axis FB
÷100×4×2000−955−2	2000	955	2	1×40=40	1×40=40	47.7	49.7	1.04	563.7	TB
÷100×4×2000−935−2	2000	935	2	2×40=80	1×40=40	47.7	48.7	1.02	569.1	TB
÷100×4×2000−935−2	2000	935	2	2×40=80	2×40=80	47.7	48.7	1.02	652.7	TB
÷100×4×2000−875−2	2000	875	2	5×40=200	2×40=80	47.7	45.6	0.95	680.9	TB
÷100×4×2000−835−2	2000	835	2	7×40=280	1×40=40	47.7	43.5	0.91	688.2	TB
÷100×4×2000−835−2	2000	835	2	7×40=280	2×40=80	47.7	43.5	0.91	695.3	TB

Table ii Geometry and failure data of duplex CFSS FE built−up columns in the parametric study.

FE model	L (mm)	a (mm)	m	EFG (mm)	IFG (mm)	L/i	a/i_i	$\frac{a/i_i}{L/i}$	$P_{u,FEM}$ (kN)	Failure mode
T60×4×1100−930−1	1100	930	1	3×40=120	N/A[1)]	42.9	85.1	1.98	234.3	FTB
T60×4×1100−465−2	1100	465	2	3×40=120	1×40=40	42.9	42.5	0.99	234.7	FTB
T60×4×1300−565−2	1300	565	2	3×40=120	1×40=40	50.7	51.7	1.02	222.4	FTB
T60×4×1500−665−2	1500	665	2	3×40=120	1×40=40	58.5	60.8	1.04	208.3	FTB
T60×4×2000−915−2	2000	915	2	3×40=120	1×40=40	78.0	83.7	1.07	158.7	FTB
T60×4×2000−625−3	2000	625	3	3×40=120	1×40=40	78.0	57.2	0.73	161.9	FTB
T60×4×2300−725−3	2300	725	3	3×40=120	1×40=40	89.7	66.3	0.74	129.5	FTB + *y*−*y* axis FB
T60×4×2900−925−3	2900	925	3	3×40=120	1×40=40	113.0	84.6	0.75	89.3	FTB + *y*−*y* axis FB
T60×4×3200−1025−3	3200	1025	3	3×40=120	1×40=40	124.7	93.8	0.75	76.9	FTB + *y*−*y* axis FB
T60×4×3800−1225−3	3800	1225	3	3×40=120	1×40=40	148.1	112.1	0.76	58.8	FTB + *y*−*y* axis FB
T60×4×4400−1425−3	4400	1425	3	3×40=120	1×40=40	171.5	130.4	0.76	47.0	FTB + *y*−*y* axis FB
T60×4×5000−1625−3	5000	1625	3	3×40=120	1×40=40	194.9	148.7	0.76	39.5	FTB + *y*−*y* axis FB
T80×4×1200−495−2	1200	495	2	4×40=160	2×40=80	35.5	32.8	0.92	226.9	FTB
T80×4×1500−645−2	1500	645	2	4×40=160	2×40=80	44.4	42.8	0.96	213.2	FTB
T80×4×1800−795−2	1800	795	2	4×40=160	2×40=80	53.3	52.7	0.99	204.8	FTB
T80×4×2100−645−3	2100	645	3	4×40=160	2×40=80	62.2	42.8	0.69	204.8	FTB
T80×4×2400−745−3	2400	745	3	4×40=160	2×40=80	71.0	49.4	0.70	198.9	FTB
T80×4×2700−845−3	2700	845	3	4×40=160	2×40=80	79.9	56.0	0.70	193.1	FTB
T80×4×3000−945−3	3000	945	3	4×40=160	2×40=80	88.8	62.7	0.71	174.4	FTB + *y*−*y* axis FB
T80×4×3300−1045−3	3300	1045	3	4×40=160	2×40=80	97.7	69.3	0.71	146.0	FTB + *y*−*y* axis FB
T80×4×3600−1145−3	3600	1145	3	4×40=160	2×40=80	106.6	75.9	0.71	131.3	FTB + *y*−*y* axis FB

T80×4×3900−1275−3	3900	1275	3	4×40=160	2×40=80	115.5	84.5	0.73	117.2	FTB + *y*−*y* axis FB
T80×4×4200−1345−3	4200	1345	3	4×40=160	2×40=80	124.3	89.2	0.72	104.3	FTB + *y*−*y* axis FB
T80×4×4600−1475−3	4600	1475	3	4×40=160	2×40=80	136.2	97.8	0.72	90.7	FTB + *y*−*y* axis FB
T80×4×4900−1575−3	4900	1575	3	4×40=160	2×40=80	145.1	104.4	0.72	81.3	FTB + *y*−*y* axis FB
T80×4×5200−1675−3	5200	1675	3	4×40=160	2×40=80	153.9	111.1	0.72	74.0	FTB + *y*−*y* axis FB
T80×4×5500−1775−3	5500	1775	3	4×40=160	2×40=80	162.8	117.7	0.72	67.6	FTB + *y*−*y* axis FB
T80×4×5800−1875−3	5800	1875	3	4×40=160	2×40=80	171.7	124.3	0.72	62.1	FTB + *y*−*y* axis FB
T100×4×1500−625−2	1500	625	2	5×40=200	2×40=80	35.8	32.5	0.91	226.4	FTB
T100×4×2500−1125−2	2500	1125	2	5×40=200	2×40=80	59.6	58.6	0.98	205.3	FTB
T100×4×2500−770−3	2500	770	3	5×40=200	2×40=80	59.6	40.1	0.67	203.8	FTB
T100×4×2800−870−3	2800	870	3	5×40=200	2×40=80	66.8	45.3	0.68	194.0	FTB
T100×4×3100−970−3	3100	970	3	5×40=200	2×40=80	73.9	50.5	0.68	171.5	FTB
T100×4×3400−1070−3	3400	1070	3	5×40=200	2×40=80	81.1	55.7	0.69	166.6	FTB
T100×4×3700−1170−3	3700	1170	3	5×40=200	2×40=80	88.3	60.9	0.69	153.9	FTB
T100×4×4000−1270−3	4000	1270	3	5×40=200	2×40=80	95.4	66.1	0.69	149.0	FTB
T100×4×4300−1370−3	4300	1370	3	5×40=200	2×40=80	102.6	71.3	0.70	143.6	FTB
T100×4×4600−1470−3	4600	1470	3	5×40=200	2×40=80	109.7	76.5	0.70	137.3	FTB
T100×4×4900−1570−3	4900	1570	3	5×40=200	2×40=80	116.9	81.7	0.70	130.9	FTB
T100×4×5200−1670−3	5200	1670	3	5×40=200	2×40=80	124.0	86.9	0.70	124.1	FTB
T100×4×5500−1770−3	5500	1770	3	5×40=200	2×40=80	131.2	92.2	0.70	117.1	FTB
T100×4×5800−1870−3	5800	1870	3	5×40=200	2×40=80	138.3	97.4	0.70	109.9	FTB
T100×4×6100−1970−3	6100	1970	3	5×40=200	2×40=80	145.5	102.6	0.70	103.0	FTB
÷60×4×1100−930−1	1100	930	1	3×40=120	N/A[1)]	42.9	85.1	1.98	550.2	TB
÷60×4×1100−465−2	1100	465	2	3×40=120	[2)]	42.9	42.5	0.99	549.5	TB
÷60×4×1300−565−2	1300	565	2	3×40=120	1×40=40	50.7	51.7	1.02	483.7	TB
÷60×4×1500−665−2	1500	665	2	3×40=120	1×40=40	58.5	60.8	1.04	467.8	TB
÷60×4×2000−915−2	2000	915	2	3×40=120	1×40=40	78.0	83.7	1.07	334.7	*u*−*u* / *v*−*v* axis FB + TB
÷60×4×2000−625−3	2000	625	3	3×40=120	1×40=40	78.0	57.2	0.73	343.1	*u*−*u* / *v*−*v* axis FB + TB
÷60×4×2300−725−3	2300	725	3	3×40=120	1×40=40	89.7	66.3	0.74	267.2	*y*−*y* / *z*−*z* axis FB
÷60×4×2900−925−3	2900	925	3	3×40=120	1×40=40	113.0	84.6	0.75	192.2	*u*−*u* / *v*−*v* axis FB
÷60×4×3200−1025−3	3200	1025	3	3×40=120	1×40=40	124.7	93.8	0.75	157.6	*u*−*u* / *v*−*v* axis FB
÷60×4×3800−1225−3	3800	1225	3	3×40=120	1×40=40	148.1	112.1	0.76	113.2	*u*−*u* / *v*−*v* axis FB
÷60×4×4400−1425−3	4400	1425	3	3×40=120	1×40=40	171.5	130.4	0.76	88.2	*u*−*u* / *v*−*v* axis FB
÷60×4×5000−1625−3	5000	1625	3	3×40=120	1×40=40	194.9	148.7	0.76	73.6	*u*−*u* / *v*−*v* axis FB
÷80×4×1200−495−2	1200	495	2	4×40=160	2×40=80	35.5	32.8	0.92	703.0	TB
÷80×4×1500−645−2	1500	645	2	4×40=160	2×40=80	44.4	42.8	0.96	619.6	TB
÷80×4×1800−795−2	1800	795	2	4×40=160	2×40=80	53.3	52.7	0.99	526.0	TB
÷80×4×2100−645−3	2100	645	3	4×40=160	2×40=80	62.2	42.8	0.69	460.7	TB
÷80×4×2400−745−3	2400	745	3	4×40=160	2×40=80	71.0	49.4	0.70	434.1	TB
÷80×4×2700−845−3	2700	845	3	4×40=160	2×40=80	79.9	56.0	0.70	411.7	TB
÷80×4×3000−945−3	3000	945	3	4×40=160	2×40=80	88.8	62.7	0.71	386.1	TB + *u*−*u* / *v*−*v* axis FB
÷80×4×3300−1045−3	3300	1045	3	4×40=160	2×40=80	97.7	69.3	0.71	344.3	TB + *u*−*u* / *v*−*v* axis FB
÷80×4×3600−1145−3	3600	1145	3	4×40=160	2×40=80	106.6	75.9	0.71	302.2	*u*−*u* / *v*−*v* axis FB + TB
÷80×4×3900−1275−3	3900	1275	3	4×40=160	2×40=80	115.5	84.5	0.73	270.0	*u*−*u* / *v*−*v* axis FB + TB
÷80×4×4200−1345−3	4200	1345	3	4×40=160	2×40=80	124.3	89.2	0.72	226.8	*u*−*u* / *v*−*v* axis FB + TB
÷80×4×4600−1475−3	4600	1475	3	4×40=160	2×40=80	136.2	97.8	0.72	191.8	*u*−*u* / *v*−*v* axis FB + TB
÷80×4×4900−1575−3	4900	1575	3	4×40=160	2×40=80	145.1	104.4	0.72	155.8	*y*−*y* / *z*−*z* axis FB + TB
÷80×4×5200−1675−3	5200	1675	3	4×40=160	2×40=80	153.9	111.1	0.72	154.3	*y*−*y* / *z*−*z* axis FB + TB
÷80×4×5500−1775−3	5500	1775	3	4×40=160	2×40=80	162.8	117.7	0.72	139.9	*u*−*u* / *v*−*v* axis FB + TB
÷80×4×5800−1875−3	5800	1875	3	4×40=160	2×40=80	171.7	124.3	0.72	130.1	*u*−*u* / *v*−*v* axis FB
÷100×4×1500−625−2	1500	625	2	5×40=200	2×40=80	35.8	32.5	0.91	825.1	TB

÷100×4×2500−1125−2	2500	1125	2	5×40=200	2×40=80	59.6	58.6	0.98	622.1	TB
÷100×4×2500−770−3	2500	770	3	5×40=200	2×40=80	59.6	40.1	0.67	645.5	TB
÷100×4×2800−870−3	2800	870	3	5×40=200	2×40=80	66.8	45.3	0.68	578.0	TB
÷100×4×3100−970−3	3100	970	3	5×40=200	2×40=80	73.9	50.5	0.68	528.3	TB
÷100×4×3400−1070−3	3400	1070	3	5×40=200	2×40=80	81.1	55.7	0.69	531.7	TB
÷100×4×3700−1170−3	3700	1170	3	5×40=200	2×40=80	88.3	60.9	0.69	531.6	TB
÷100×4×4000−1270−3	4000	1270	3	5×40=200	2×40=80	95.4	66.1	0.69	496.4	TB
÷100×4×4300−1370−3	4300	1370	3	5×40=200	2×40=80	102.6	71.3	0.70	420.0	TB
÷100×4×4600−1470−3	4600	1470	3	5×40=200	2×40=80	109.7	76.5	0.70	333.2	TB
÷100×4×4900−1570−3	4900	1570	3	5×40=200	2×40=80	116.9	81.7	0.70	311.5	TB
÷100×4×5200−1670−3	5200	1670	3	5×40=200	2×40=80	124.0	86.9	0.70	292.6	TB + *u*−*u* / *v*−*v* axis FB
÷100×4×5500−1770−3	5500	1770	3	5×40=200	2×40=80	131.2	92.2	0.70	267.9	*u*−*u* / *v*−*v* axis FB + TB
÷100×4×5800−1870−3	5800	1870	3	5×40=200	2×40=80	138.3	97.4	0.70	247.0	*u*−*u* / *v*−*v* axis FB + TB
÷100×4×6100−1970−3	6100	1970	3	5×40=200	2×40=80	145.5	102.6	0.70	215.3	*y*−*y* / *z*−*z* axis FB + TB

[1)] Columns without IFG.
[2)] One bolt on each connected legs in the interconnections.

1 **Table iii Geometry and failure data of austenitic CFSS FE built-up columns in the parametric study.**

FE model	L (mm)	a (mm)	m	EFG (mm)	IFG (mm)	L/i	a/i_i	$\frac{a/i_i}{L/i}$	$P_{u,FEM}$ (kN)	Failure mode
T60×4×1100−930−1	1100	930	1	3×40=120	N/A[1)]	42.9	10.9	0.25	159.7	FTB
T60×4×1100−465−2	1100	465	2	3×40=120	[2)]	42.9	10.9	0.25	158.7	FTB
T60×4×1300−565−2	1300	565	2	3×40=120	1×40=40	50.7	10.9	0.22	160.7	FTB
T60×4×1500−665−2	1500	665	2	3×40=120	1×40=40	58.5	10.9	0.19	150.5	FTB
T60×4×2000−915−2	2000	915	2	3×40=120	1×40=40	78.0	10.9	0.14	134.0	FTB
T60×4×2000−625−3	2000	625	3	3×40=120	1×40=40	78.0	10.9	0.14	136.1	FTB
T60×4×2300−725−3	2300	725	3	3×40=120	1×40=40	89.7	10.9	0.12	120.5	FTB + *y*−*y* axis FB
T60×4×2900−925−3	2900	925	3	3×40=120	1×40=40	113.0	10.9	0.10	88.6	FTB + *y*−*y* axis FB
T60×4×3200−1025−3	3200	1025	3	3×40=120	1×40=40	124.7	10.9	0.09	76.5	FTB + *y*−*y* axis FB
T60×4×3800−1225−3	3800	1225	3	3×40=120	1×40=40	148.1	10.9	0.07	58.8	FTB + *y*−*y* axis FB
T60×4×4400−1425−3	4400	1425	3	3×40=120	1×40=40	171.5	10.9	0.06	47.0	FTB + *y*−*y* axis FB
T60×4×5000−1625−3	5000	1625	3	3×40=120	1×40=40	194.9	10.9	0.06	39.5	FTB + *y*−*y* axis FB
T80×4×1000−395−2	1000	395	2	4×40=160	2×40=80	29.6	26.2	0.88	209.3	FTB
T80×4×1200−495−2	1200	495	2	4×40=160	2×40=80	35.5	32.8	0.92	193.1	FTB
T80×4×1500−645−2	1500	645	2	4×40=160	2×40=80	44.4	42.8	0.96	188.7	FTB
T80×4×1800−795−2	1800	795	2	4×40=160	2×40=80	53.3	52.7	0.99	185.2	FTB
T80×4×2100−645−3	2100	645	3	4×40=160	2×40=80	62.2	42.8	0.69	182.3	FTB
T80×4×2400−745−3	2400	745	3	4×40=160	2×40=80	71.0	49.4	0.70	175.4	FTB
T80×4×2700−845−3	2700	845	3	4×40=160	2×40=80	79.9	56.0	0.70	166.0	FTB + *y*−*y* axis FB
T80×4×3000−945−3	3000	945	3	4×40=160	2×40=80	88.8	62.7	0.71	153.9	FTB + *y*−*y* axis FB
T80×4×3300−1045−3	3300	1045	3	4×40=160	2×40=80	97.7	69.3	0.71	140.9	FTB + *y*−*y* axis FB
T80×4×3600−1145−3	3600	1145	3	4×40=160	2×40=80	106.6	75.9	0.71	128.4	FTB + *y*−*y* axis FB
T80×4×3900−1275−3	3900	1275	3	4×40=160	2×40=80	115.5	84.5	0.73	115.6	FTB + *y*−*y* axis FB
T80×4×4200−1345−3	4200	1345	3	4×40=160	2×40=80	124.3	89.2	0.72	103.9	FTB + *y*−*y* axis FB
T80×4×4600−1475−3	4600	1475	3	4×40=160	2×40=80	136.2	97.8	0.72	90.2	FTB + *y*−*y* axis FB
T80×4×4900−1575−3	4900	1575	3	4×40=160	2×40=80	145.1	104.4	0.72	81.3	FTB + *y*−*y* axis FB
T80×4×5200−1675−3	5200	1675	3	4×40=160	2×40=80	153.9	111.1	0.72	74.0	FTB + *y*−*y* axis FB
T80×4×5500−1775−3	5500	1775	3	4×40=160	2×40=80	162.8	117.7	0.72	67.6	FTB + *y*−*y* axis FB
T80×4×5800−1875−3	5800	1875	3	4×40=160	2×40=80	171.7	124.3	0.72	62.1	FTB + *y*−*y* axis FB
T80×4×6000−1970−3	6000	1970	3	4×40=160	2×40=80	177.6	130.6	0.74	58.8	FTB + *y*−*y* axis FB
T100×4×1500−625−2	1500	625	2	5×40=200	2×40=80	35.8	32.5	0.91	183.3	FTB
T100×4×2000−875−2	2000	875	2	5×40=200	2×40=80	47.7	45.6	0.95	174.6	FTB
T100×4×2500−1125−2	2500	1125	2	5×40=200	2×40=80	59.6	58.6	0.98	167.8	FTB
T100×4×2500−770−3	2500	770	3	5×40=200	2×40=80	59.6	40.1	0.67	170.0	FTB
T100×4×2800−870−3	2800	870	3	5×40=200	2×40=80	66.8	45.3	0.68	166.1	FTB
T100×4×3100−970−3	3100	970	3	5×40=200	2×40=80	73.9	50.5	0.68	162.7	FTB

T100×4×3400−1070−3	3400	1070	3	5×40=200	2×40=80	81.1	55.7	0.69	158.3	FTB
T100×4×3700−1170−3	3700	1170	3	5×40=200	2×40=80	88.3	60.9	0.69	153.9	FTB
T100×4×4000−1270−3	4000	1270	3	5×40=200	2×40=80	95.4	66.1	0.69	149.0	FTB
T100×4×4300−1370−3	4300	1370	3	5×40=200	2×40=80	102.6	71.3	0.70	143.6	FTB
T100×4×4600−1470−3	4600	1470	3	5×40=200	2×40=80	109.7	76.5	0.70	137.3	FTB
T100×4×4900−1570−3	4900	1570	3	5×40=200	2×40=80	116.9	81.7	0.70	130.9	FTB
T100×4×5200−1670−3	5200	1670	3	5×40=200	2×40=80	124.0	86.9	0.70	124.1	FTB
T100×4×5500−1770−3	5500	1770	3	5×40=200	2×40=80	131.2	92.2	0.70	117.1	FTB
T100×4×5800−1870−3	5800	1870	3	5×40=200	2×40=80	138.3	97.4	0.70	109.9	FTB
T100×4×6100−1970−3	6100	1970	3	5×40=200	2×40=80	145.5	102.6	0.70	103.0	FTB
÷60×4×1100−930−1	1100	930	1	3×40=120	N/A[1)]	42.9	85.1	1.98	390.4	TB
÷60×4×1100−465−2	1100	465	2	3×40=120	[2)]	42.9	42.5	0.99	389.9	TB
÷60×4×1300−565−2	1300	565	2	3×40=120	1×40=40	50.7	51.7	1.02	383.0	TB
÷60×4×1500−665−2	1500	665	2	3×40=120	1×40=40	58.5	60.8	1.04	365.0	TB
÷60×4×2000−915−2	2000	915	2	3×40=120	1×40=40	78.0	83.7	1.07	255.2	*u*−*u* / *v*−*v* axis FB + TB
÷60×4×2000−625−3	2000	625	3	3×40=120	1×40=40	78.0	57.2	0.73	260.9	*u*−*u* / *v*−*v* axis FB + TB
÷60×4×2300−725−3	2300	725	3	3×40=120	1×40=40	89.7	66.3	0.74	216.6	*y*−*y* / *z*−*z* axis FB
÷60×4×2900−925−3	2900	925	3	3×40=120	1×40=40	113.0	84.6	0.75	177.6	*u*−*u* / *v*−*v* axis FB
÷60×4×3200−1025−3	3200	1025	3	3×40=120	1×40=40	124.7	93.8	0.75	152.1	*u*−*u* / *v*−*v* axis FB
÷60×4×3800−1225−3	3800	1225	3	3×40=120	1×40=40	148.1	112.1	0.76	112.8	*u*−*u* / *v*−*v* axis FB
÷60×4×4400−1425−3	4400	1425	3	3×40=120	1×40=40	171.5	130.4	0.76	88.2	*u*−*u* / *v*−*v* axis FB
÷60×4×5000−1625−3	5000	1625	3	3×40=120	1×40=40	194.9	148.7	0.76	73.6	*u*−*u* / *v*−*v* axis FB
÷80×4×1000−395−2	1000	395	2	4×40=160	2×40=80	29.6	26.2	0.88	481.3	TB
÷80×4×1200−495−2	1200	495	2	4×40=160	2×40=80	35.5	32.8	0.92	460.7	TB
÷80×4×1500−645−2	1500	645	2	4×40=160	2×40=80	44.4	42.8	0.96	426.2	TB
÷80×4×1800−795−2	1800	795	2	4×40=160	2×40=80	53.3	52.7	0.99	393.8	TB
÷80×4×2100−645−3	2100	645	3	4×40=160	2×40=80	62.2	42.8	0.69	373.7	TB
÷80×4×2400−745−3	2400	745	3	4×40=160	2×40=80	71.0	49.4	0.70	367.9	TB
÷80×4×2700−845−3	2700	845	3	4×40=160	2×40=80	79.9	56.0	0.70	364.2	TB
÷80×4×3000−945−3	3000	945	3	4×40=160	2×40=80	88.8	62.7	0.71	342.9	TB + *u*−*u* / *v*−*v* axis FB
÷80×4×3300−1045−3	3300	1045	3	4×40=160	2×40=80	97.7	69.3	0.71	312.9	TB + *u*−*u* / *v*−*v* axis FB
÷80×4×3600−1145−3	3600	1145	3	4×40=160	2×40=80	106.6	75.9	0.71	277.3	*u*−*u* / *v*−*v* axis FB + TB
÷80×4×3900−1275−3	3900	1275	3	4×40=160	2×40=80	115.5	84.5	0.73	257.4	*u*−*u* / *v*−*v* axis FB + TB
÷80×4×4200−1345−3	4200	1345	3	4×40=160	2×40=80	124.3	89.2	0.72	219.2	*u*−*u* / *v*−*v* axis FB + TB
÷80×4×4600−1475−3	4600	1475	3	4×40=160	2×40=80	136.2	97.8	0.72	189.3	*u*−*u* / *v*−*v* axis FB + TB
÷80×4×4900−1575−3	4900	1575	3	4×40=160	2×40=80	145.1	104.4	0.72	153.3	*y*−*y* / *z*−*z* axis FB + TB
÷80×4×5200−1675−3	5200	1675	3	4×40=160	2×40=80	153.9	111.1	0.72	154.3	*y*−*y* / *z*−*z* axis FB + TB
÷80×4×5500−1775−3	5500	1775	3	4×40=160	2×40=80	162.8	117.7	0.72	139.9	*u*−*u* / *v*−*v* axis FB + TB
÷80×4×5800−1875−3	5800	1875	3	4×40=160	2×40=80	171.7	124.3	0.72	130.1	*u*−*u* / *v*−*v* axis FB
÷80×4×6000−1970−3	6000	1970	3	4×40=160	2×40=80	177.6	130.6	0.74	123.9	*u*−*u* / *v*−*v* axis FB
÷100×4×1500−625−2	1500	625	2	5×40=200	2×40=80	35.8	32.5	0.91	544.4	TB
÷100×4×2000−875−2	2000	875	2	5×40=200	2×40=80	47.7	45.6	0.95	467.1	TB
÷100×4×2500−1125−2	2500	1125	2	5×40=200	2×40=80	59.6	58.6	0.98	411.5	TB
÷100×4×2500−770−3	2500	770	3	5×40=200	2×40=80	59.6	40.1	0.67	391.7	TB
÷100×4×2800−870−3	2800	870	3	5×40=200	2×40=80	66.8	45.3	0.68	371.2	TB
÷100×4×3100−970−3	3100	970	3	5×40=200	2×40=80	73.9	50.5	0.68	341.6	TB
÷100×4×3400−1070−3	3400	1070	3	5×40=200	2×40=80	81.1	55.7	0.69	338.4	TB
÷100×4×3700−1170−3	3700	1170	3	5×40=200	2×40=80	88.3	60.9	0.69	335.4	TB
÷100×4×4000−1270−3	4000	1270	3	5×40=200	2×40=80	95.4	66.1	0.69	333.1	TB
÷100×4×4300−1370−3	4300	1370	3	5×40=200	2×40=80	102.6	71.3	0.70	327.0	TB
÷100×4×4600−1470−3	4600	1470	3	5×40=200	2×40=80	109.7	76.5	0.70	320.6	TB
÷100×4×4900−1570−3	4900	1570	3	5×40=200	2×40=80	116.9	81.7	0.70	305.8	TB
÷100×4×5200−1670−3	5200	1670	3	5×40=200	2×40=80	124.0	86.9	0.70	288.3	TB + *u*−*u* / *v*−*v* axis FB
÷100×4×5500−1770−3	5500	1770	3	5×40=200	2×40=80	131.2	92.2	0.70	265.2	*u*−*u* / *v*−*v* axis FB + TB

÷100×4×5800−1870−3	5800	1870	3	5×40=200	2×40=80	138.3	97.4	0.70	246.4	*u*−*u* / *v*−*v* axis FB + TB
÷100×4×6100−1970−3	6100	1970	3	5×40=200	2×40=80	145.5	102.6	0.70	212.9	*y*−*y* / *z*−*z* axis FB + TB
[1)] Column without IFG.										
[2)] One bolt on each connected legs in the interconnections.										

1 **Table iv Geometry and failure data of ferritic CFSS FE built−up columns in the parametric study.**

FE model	*L* (mm)	*a* (mm)	*m*	EFG (mm)	IFG (mm)	*L*/*i*	*a*/i_i	$\frac{a/i_i}{L/i}$	$P_{u,FEM}$ (kN)	Failure mode
T60×4×1100−930−1	1100	930	1	3×40=120	N/A[1)]	42.9	85.1	1.98	222.5	FTB
T60×4×1100−465−2	1100	465	2	3×40=120	[2)]	42.9	42.5	0.99	223.2	FTB
T60×4×1300−565−2	1300	565	2	3×40=120	1×40=40	50.7	51.7	1.02	206.0	FTB
T60×4×1500−665−2	1500	665	2	3×40=120	1×40=40	58.5	60.8	1.04	197.4	FTB
T60×4×2000−915−2	2000	915	2	3×40=120	1×40=40	78.0	83.7	1.07	152.9	FTB
T60×4×2000−625−3	2000	625	3	3×40=120	1×40=40	78.0	57.2	0.73	157.0	FTB
T60×4×2300−725−3	2300	725	3	3×40=120	1×40=40	89.7	66.3	0.74	128.1	FTB + *y*−*y* axis FB
T60×4×2900−925−3	2900	925	3	3×40=120	1×40=40	113.0	84.6	0.75	89.2	FTB + *y*−*y* axis FB
T60×4×3200−1025−3	3200	1025	3	3×40=120	1×40=40	124.7	93.8	0.75	76.9	FTB + *y*−*y* axis FB
T60×4×3800−1225−3	3800	1225	3	3×40=120	1×40=40	148.1	112.1	0.76	58.8	FTB + *y*−*y* axis FB
T60×4×4400−1425−3	4400	1425	3	3×40=120	1×40=40	171.5	130.4	0.76	47.0	FTB + *y*−*y* axis FB
T60×4×5000−1625−3	5000	1625	3	3×40=120	1×40=40	194.9	148.7	0.76	39.5	FTB + *y*−*y* axis FB
T80×4×1000−395−2	1000	395	2	4×40=160	2×40=80	29.6	26.2	0.88	262.6	FTB
T80×4×1200−495−2	1200	495	2	4×40=160	2×40=80	35.5	32.8	0.92	219.3	FTB
T80×4×1500−645−2	1500	645	2	4×40=160	2×40=80	44.4	42.8	0.96	205.8	FTB
T80×4×1800−795−2	1800	795	2	4×40=160	2×40=80	53.3	52.7	0.99	198.9	FTB
T80×4×2100−645−3	2100	645	3	4×40=160	2×40=80	62.2	42.8	0.69	198.9	FTB
T80×4×2400−745−3	2400	745	3	4×40=160	2×40=80	71.0	49.4	0.70	188.2	FTB
T80×4×2700−845−3	2700	845	3	4×40=160	2×40=80	79.9	56.0	0.70	175.4	FTB + *y*−*y* axis FB
T80×4×3000−945−3	3000	945	3	4×40=160	2×40=80	88.8	62.7	0.71	159.7	FTB + *y*−*y* axis FB
T80×4×3300−1045−3	3300	1045	3	4×40=160	2×40=80	97.7	69.3	0.71	145.5	FTB + *y*−*y* axis FB
T80×4×3600−1145−3	3600	1145	3	4×40=160	2×40=80	106.6	75.9	0.71	130.8	FTB + *y*−*y* axis FB
T80×4×3900−1275−3	3900	1275	3	4×40=160	2×40=80	115.5	84.5	0.73	117.1	FTB + *y*−*y* axis FB
T80×4×4200−1345−3	4200	1345	3	4×40=160	2×40=80	124.3	89.2	0.72	103.9	FTB + *y*−*y* axis FB
T80×4×4600−1475−3	4600	1475	3	4×40=160	2×40=80	136.2	97.8	0.72	90.2	FTB + *y*−*y* axis FB
T80×4×4900−1575−3	4900	1575	3	4×40=160	2×40=80	145.1	104.4	0.72	81.3	FTB + *y*−*y* axis FB
T80×4×5200−1675−3	5200	1675	3	4×40=160	2×40=80	153.9	111.1	0.72	74.0	FTB + *y*−*y* axis FB
T80×4×5500−1775−3	5500	1775	3	4×40=160	2×40=80	162.8	117.7	0.72	67.6	FTB + *y*−*y* axis FB
T80×4×5800−1875−3	5800	1875	3	4×40=160	2×40=80	171.7	124.3	0.72	62.1	FTB + *y*−*y* axis FB
T80×4×6000−1970−3	6000	1970	3	4×40=160	2×40=80	177.6	130.6	0.74	58.8	FTB + *y*−*y* axis FB
T100×4×1500−625−2	1500	625	2	5×40=200	2×40=80	35.8	32.5	0.91	212.9	FTB
T100×4×2000−875−2	2000	875	2	5×40=200	2×40=80	47.7	45.6	0.95	200.9	FTB
T100×4×2500−1125−2	2500	1125	2	5×40=200	2×40=80	59.6	58.6	0.98	182.8	FTB
T100×4×2500−770−3	2500	770	3	5×40=200	2×40=80	59.6	40.1	0.67	192.1	FTB
T100×4×2800−870−3	2800	870	3	5×40=200	2×40=80	66.8	45.3	0.68	184.2	FTB
T100×4×3100−970−3	3100	970	3	5×40=200	2×40=80	73.9	50.5	0.68	166.6	FTB
T100×4×3400−1070−3	3400	1070	3	5×40=200	2×40=80	81.1	55.7	0.69	158.8	FTB
T100×4×3700−1170−3	3700	1170	3	5×40=200	2×40=80	88.3	60.9	0.69	153.9	FTB
T100×4×4000−1270−3	4000	1270	3	5×40=200	2×40=80	95.4	66.1	0.69	149.0	FTB
T100×4×4300−1370−3	4300	1370	3	5×40=200	2×40=80	102.6	71.3	0.70	143.6	FTB
T100×4×4600−1470−3	4600	1470	3	5×40=200	2×40=80	109.7	76.5	0.70	137.3	FTB
T100×4×4900−1570−3	4900	1570	3	5×40=200	2×40=80	116.9	81.7	0.70	130.9	FTB
T100×4×5200−1670−3	5200	1670	3	5×40=200	2×40=80	124.0	86.9	0.70	124.1	FTB
T100×4×5500−1770−3	5500	1770	3	5×40=200	2×40=80	131.2	92.2	0.70	117.1	FTB
T100×4×5800−1870−3	5800	1870	3	5×40=200	2×40=80	138.3	97.4	0.70	109.9	FTB
T100×4×6100−1970−3	6100	1970	3	5×40=200	2×40=80	145.5	102.	0.70	103.0	FTB

							6			
÷60×4×1100−930−1	1100	930	1	3×40=120	N/A[1)]	42.9	85.1	1.98	473.5	TB
÷60×4×1100−465−2	1100	465	2	3×40=120	[2)]	42.9	42.5	0.99	472.0	TB
÷60×4×1300−565−2	1300	565	2	3×40=120	1×40=40	50.7	51.7	1.02	461.6	TB
÷60×4×1500−665−2	1500	665	2	3×40=120	1×40=40	58.5	60.8	1.04	459.0	TB
÷60×4×2000−915−2	2000	915	2	3×40=120	1×40=40	78.0	83.7	1.07	310.9	*u*−*u* / *v*−*v* axis FB + TB
÷60×4×2000−625−3	2000	625	3	3×40=120	1×40=40	78.0	57.2	0.73	318.8	*u*−*u* / *v*−*v* axis FB + TB
÷60×4×2300−725−3	2300	725	3	3×40=120	1×40=40	89.7	66.3	0.74	254.3	*y*−*y* / *z*−*z* axis FB
÷60×4×2900−925−3	2900	925	3	3×40=120	1×40=40	113.0	84.6	0.75	188.3	*u*−*u* / *v*−*v* axis FB
÷60×4×3200−1025−3	3200	1025	3	3×40=120	1×40=40	124.7	93.8	0.75	156.4	*u*−*u* / *v*−*v* axis FB
÷60×4×3800−1225−3	3800	1225	3	3×40=120	1×40=40	148.1	112.1	0.76	113.2	*u*−*u* / *v*−*v* axis FB
÷60×4×4400−1425−3	4400	1425	3	3×40=120	1×40=40	171.5	130.4	0.76	88.2	*u*−*u* / *v*−*v* axis FB
÷60×4×5000−1625−3	5000	1625	3	3×40=120	1×40=40	194.9	148.7	0.76	73.6	*u*−*u* / *v*−*v* axis FB
÷80×4×1000−395−2	1000	395	2	4×40=160	2×40=80	29.6	26.2	0.88	521.1	TB
÷80×4×1200−495−2	1200	495	2	4×40=160	2×40=80	35.5	32.8	0.92	505.1	TB
÷80×4×1500−645−2	1500	645	2	4×40=160	2×40=80	44.4	42.8	0.96	475.7	TB
÷80×4×1800−795−2	1800	795	2	4×40=160	2×40=80	53.3	52.7	0.99	446.7	TB
÷80×4×2100−645−3	2100	645	3	4×40=160	2×40=80	62.2	42.8	0.69	416.4	TB
÷80×4×2400−745−3	2400	745	3	4×40=160	2×40=80	71.0	49.4	0.70	405.8	TB
÷80×4×2700−845−3	2700	845	3	4×40=160	2×40=80	79.9	56.0	0.70	397.3	TB
÷80×4×3000−945−3	3000	945	3	4×40=160	2×40=80	88.8	62.7	0.71	375.9	TB + *u*−*u* / *v*−*v* axis FB
÷80×4×3300−1045−3	3300	1045	3	4×40=160	2×40=80	97.7	69.3	0.71	337.3	TB + *u*−*u* / *v*−*v* axis FB
÷80×4×3600−1145−3	3600	1145	3	4×40=160	2×40=80	106.6	75.9	0.71	296.4	*u*−*u* / *v*−*v* axis FB + TB
÷80×4×3900−1275−3	3900	1275	3	4×40=160	2×40=80	115.5	84.5	0.73	268.0	*u*−*u* / *v*−*v* axis FB + TB
÷80×4×4200−1345−3	4200	1345	3	4×40=160	2×40=80	124.3	89.2	0.72	225.3	*u*−*u* / *v*−*v* axis FB + TB
÷80×4×4600−1475−3	4600	1475	3	4×40=160	2×40=80	136.2	97.8	0.72	191.4	*u*−*u* / *v*−*v* axis FB + TB
÷80×4×4900−1575−3	4900	1575	3	4×40=160	2×40=80	145.1	104.4	0.72	155.3	*y*−*y* / *z*−*z* axis FB + TB
÷80×4×5200−1675−3	5200	1675	3	4×40=160	2×40=80	153.9	111.1	0.72	154.3	*y*−*y* / *z*−*z* axis FB + TB
÷80×4×5500−1775−3	5500	1775	3	4×40=160	2×40=80	162.8	117.7	0.72	139.9	*u*−*u* / *v*−*v* axis FB + TB
÷80×4×5800−1875−3	5800	1875	3	4×40=160	2×40=80	171.7	124.3	0.72	130.1	*u*−*u* / *v*−*v* axis FB
÷80×4×6000−1970−3	6000	1970	3	4×40=160	2×40=80	177.6	130.6	0.74	123.9	*u*−*u* / *v*−*v* axis FB
÷100×4×1500−625−2	1500	625	2	5×40=200	2×40=80	35.8	32.5	0.91	591.4	TB
÷100×4×2000−875−2	2000	875	2	5×40=200	2×40=80	47.7	45.6	0.95	525.9	TB
÷100×4×2500−1125−2	2500	1125	2	5×40=200	2×40=80	59.6	58.6	0.98	465.1	TB
÷100×4×2500−770−3	2500	770	3	5×40=200	2×40=80	59.6	40.1	0.67	462.4	TB
÷100×4×2800−870−3	2800	870	3	5×40=200	2×40=80	66.8	45.3	0.68	443.9	TB
÷100×4×3100−970−3	3100	970	3	5×40=200	2×40=80	73.9	50.5	0.68	361.3	TB
÷100×4×3400−1070−3	3400	1070	3	5×40=200	2×40=80	81.1	55.7	0.69	429.8	TB
÷100×4×3700−1170−3	3700	1170	3	5×40=200	2×40=80	88.3	60.9	0.69	414.0	TB
÷100×4×4000−1270−3	4000	1270	3	5×40=200	2×40=80	95.4	66.1	0.69	391.6	TB
÷100×4×4300−1370−3	4300	1370	3	5×40=200	2×40=80	102.6	71.3	0.70	346.4	TB
÷100×4×4600−1470−3	4600	1470	3	5×40=200	2×40=80	109.7	76.5	0.70	331.2	TB
÷100×4×4900−1570−3	4900	1570	3	5×40=200	2×40=80	116.9	81.7	0.70	310.7	TB
÷100×4×5200−1670−3	5200	1670	3	5×40=200	2×40=80	124.0	86.9	0.70	292.0	TB + *u*−*u* / *v*−*v* axis FB
÷100×4×5500−1770−3	5500	1770	3	5×40=200	2×40=80	131.2	92.2	0.70	267.7	*u*−*u* / *v*−*v* axis FB + TB
÷100×4×5800−1870−3	5800	1870	3	5×40=200	2×40=80	138.3	97.4	0.70	247.0	*u*−*u* / *v*−*v* axis FB + TB
÷100×4×6100−1970−3	6100	1970	3	5×40=200	2×40=80	145.5	102.6	0.70	215.0	*y*−*y* / *z*−*z* axis FB + TB

[1)] Column without IFG.
[2)] One bolt on each connected legs in the interconnections.

1